Authigenic $^{10}Be/^{9}Be$ ratios and ^{10}Be-fluxes ($^{230}Th_{xs}$-normalized) in central Baffin Bay sediments during the last glacial cycle: paleoenvironmental implications

Quentin Simon,[1,*], Nicolas Thouveny[1], Didier L. Bourlès[1], Laurence Nuttin[2], Claude Hillaire-Marcel[2], Guillaume St-Onge[2,3]

[1]Aix-Marseille Université, CNRS, IRD, CEREGE UM34, 13545 Aix en Provence, France

[2]GEOTOP Research Center, H3C3P8 Montréal, Canada

[3]Institut des sciences de la mer de Rimouski (ISMER), Canada Research Chair in Marine Geology, Université du Québec à Rimouski

*simon@cerege.fr

Abstract

Authigenic $^{10}Be/^{9}Be$ ratios and ^{10}Be-fluxes reconstructed using the $^{230}Th_{xs}$ normalization, proxies of the cosmogenic radionuclide ^{10}Be production rate in the atmosphere, have been measured in a sedimentary core from Baffin Bay (North Atlantic) in order to reconstruct the geomagnetic dipole moment variations during the last ca. 136 ka BP, and for comparison with the relative paleointensity (RPI) record derived from paleomagnetic measurements. Our study revealed that the exchangeable (authigenic) ^{10}Be measured includes a strong climatic component related to the glacial dynamics that characterized the circum Baffin Bay during the last glacial period. Despite normalization applied on the authigenic ^{10}Be concentrations using both the scavenged ^{9}Be and $^{230}Th_{xs}$ approaches, a strong climatic signal still prevails. Both normalization methods yield equivalent results that are both strongly correlated with sedimentological parameters (grain-size and mineralogy). The lower $^{10}Be/^{9}Be$ ratio values are associated with coarse-grained carbonate-rich layers while the higher $^{10}Be/^{9}Be$ ratio values are found with fine-grained felspar-rich sediments. This variability is due to both i) sediment composition control over beryllium-scavenging rates, ii) the glacial history that contributed to modify the ^{10}Be concentration in the oceanic realm and notably boundary scavenging conditions. No pristine geomagnetic field intensity can thus be derived from ^{10}Be measurements in such a high-variability glacio-marine environment. These results also

indicate that the straightforward interpretation of ^{10}Be-concentration variations as a proxy of the Interglacial/Glacial (or major interstadials) cycles in Arctic and sub-Arctic regions must be considered with caution and rather propose to relate ^{10}Be variations to higher-frequency paleoclimatic changes and glacial dynamics.

1. Introduction

The cosmogenic nuclide Beryllium-10 (^{10}Be) is produced in the stratosphere (~65%) and the troposphere (~35%) by spallation reactions when highly energetic galactic cosmic rays interact with nitrogen and oxygen atoms (Lal and Peters, 1967; Dunai and Lifton, 2014). Its production rate is linked to the Sun and Earth magnetic fields variabilities by a non-linear inverse relationship (Elsasser et al., 1956; Lal, 1988; Beer et al., 1990; Masarik and Beer, 2009; Kovaltsov and Usoskin, 2010). After its production in the atmosphere, ^{10}Be is quickly scavenged onto aerosol particles themselves precipitated (or thrown) within *ca.* 1-3 years into ocean/continent reservoirs by wet or dry deposition processes (Raisbeck *et al.*, 1981; Beer et al., 1990; Baroni *et al.*, 2011). Previous studies have shown that -while solar activity inflects the production rate on shorter timescales- ^{10}Be flux measured along ice and marine sediment sequences reflect long term signatures of the geomagnetic dipole moment (Raisbeck *et al.*, 1981, 1985; Yiou *et al.*, 1985; Wagner *et al.*, 2000; Frank et al. 1997; Carcaillet et al., 2003, 2004, Muscheler *et al.* 2004, 2005). The exchangeable-^{10}Be concentrations (*i.e.*, fraction adsorbed onto settling particles) measured in the sediments, henceforth referred to the authigenic ^{10}Be, are not only reflecting the atmospheric production at the time of their deposition but also depend on the scavenging rates from the overlying water column, to advected ^{10}Be fraction due to oceanic mixing and/or to inherited ^{10}Be fraction scavenged during the terrestrial/glacial/meltwater cycling of the carrier particles. Therefore, normalization of the authigenic ^{10}Be concentration is a first step in order to remove these environmental biases and compare ^{10}Be records with geomagnetic variability.

Two methods of normalization have been used in literature: (1) normalization of the authigenic ^{10}Be cosmogenic nuclide by the authigenic stable ^{9}Be isotope supplied by terrigenous material entering the ocean (*i.e.*, originating from the dissolution of detrital, aeolian, riverine and glacier inputs). This method relies on the similar behavior of both isotopes once homogenized in seawater (Bourlès *et al.*, 1989; Brown *et al.*, 1992). The authigenic ^{10}Be/^{9}Be ratio method reliably corrects for ocean/continent secondary contributions and provides robust results clearly demonstrating an inverse relationship with the geomagnetic field (Henken-Mellies *et al.*, 1990; Robinson *et al.*, 1995; Carcaillet *et al.*, 2003, 2004a, 2004b; Thouveny *et al.*, 2008; Ménabréaz *et al.*, 2011, 2012, 2014; Valet *et al.*, 2014). The second normalization process (2) uses the ^{230}Th-excess method proposed by Bacon (1984) to calculate vertical fluxes of any sedimentary component deposited during the Late Quaternary (see François *et al.*, 2004 for a review) and has been used successfully to calculate ^{10}Be-fluxes in numerous studies (*e.g.*, Franck *et al.*, 1997, 2000; Christl *et al.*, 2007, 2010). All these studies notably demonstrate that during periods characterized by low dipole strength (*i.e.*, corresponding to episodes of collapsed field during reversals or excursions), the atmospheric ^{10}Be production rates were significantly larger than during periods with high dipole strength. Accordingly, the reconstruction of atmospheric ^{10}Be production rate signals from marine sedimentary sequences constitutes a complementary approach, independent from paleomagnetism, to decipher past geomagnetic dipole moment variations. Furthermore, the comparison between the ^{10}Be signals from mid-to-low-latitude sites (Ménabréaz *et al.*, 2012, 2014) as well as with recent simulations using general circulation models (GCMs; Heikkilä *et al.*, 2009, 2013) demonstrate a rapid zonal atmospheric mixing of ^{10}Be before its deposition in geological archives.

In the Arctic Ocean where most dating methods encounter serious limitations, the radioactive decay rates of the ^{10}Be measured in marine sediments have been used to establish a Neogene

chronostratigraphic framework (assuming a near constant supply of ^{10}Be in first approximation) of the ACEX long sedimentary sequence (Frank et al., 2008). Besides, variations in ^{10}Be concentrations in Arctic and sub-Arctic sediments have also been used in order to constrain the stratigraphy of Late Quaternary sedimentary records assuming that variations of ^{10}Be concentrations roughly represent Glacial/Interglacial cycles or major Interstadial periods (Spielhagen et al., 1997, 2004; Sellén et al., 2009; Alexanderson et al., 2014). In this mechanism, the low ^{10}Be concentrations corresponding to glacial periods are caused by a combination of: (1) low inputs of ^{10}Be due to increased sea ice cover and, (2) ^{10}Be dilution related to higher accumulation rates of ice rafted debris (IRD); and vice versa for interglacial (major interstadial) periods.

In this study, we present new authigenic ^{10}Be/^{9}Be ratios and $^{230}Th_{xs}$-normalized ^{10}Be-fluxes from a high-latitude marine record (HU2008-029-016PC) from central Baffin Bay and spanning the last 136 ka. This paper includes a revision of the initial chronostratigraphy of the core (Simon et al., 2012) in order to improve the robustness of the chronology for the bottom-half of the core. A primary aim of the study was to examine if ^{10}Be originating from continental inputs or advected through oceanic circulation and glacial processes could be removed from the total authigenic ^{10}Be concentrations by means of normalization procedures before any geomagnetic interpretations. We compare the two existing normalization methods (*i.e.*, authigenic ^{9}Be and $^{230}Th_{xs}$) using a U and Th-series isotope record from the same core (Nuttin and Hillaire-Marcel, 2015) and discuss ^{10}Be-systematics *vs.* sedimentological parameters, geomagnetic dipole moment variations, ^{10}Be-fluxes from models and marine/ice records, and, finally, we discuss its paleoenvironmental implications.

2. Environmental setting

Baffin Bay is a subpolar oceanic basin (1300 km long and 450 km wide, ~690 000 km^2) located in the northwest North Atlantic (Figure 1). The bay is one of the main export routes of

freshwater from Greenland, the canadian Arctic and the Arctic Ocean into the North Atlantic Ocean. Its morphology consists of an elongated abyssal plain (2000–2500 m) surrounded by the continental shelves of Greenland and Baffin Island. During the glacial periods, the northeastern Laurentide Ice Sheet (LIS), the Innuitian Ice Sheet (IIS) and the Greenland Ice Sheet (GIS) formed a nearly continuous and highly dynamic ice belt surrounding Baffin Bay (Figure 1). On the Greenland side, the GIS extended westward over the inner shelf, and as far as the shelf edge off Disko Bugt and the Uummannaq Trough during the Last Glacial Maximum (LGM) (Ó Cofaigh *et al.*, 2012, 2013; Funder *et al.*, 2011). The LIS extended through Baffin Island, probably as far as its fjord mouths and inlets, and possibly over part of the Baffin Island shelf during glacial maxima (Margold *et al.*, 2015). In the northern end of the bay, ice streams in the Smith Sound and Lancaster sounds were particularly large and active (England *et al.*, 2006; Klassen and Fisher, 1988; Li *et al.*, 2011) and probably developed into an ice shelf towards the bay (Alley *et al.*, 2010; Marcott *et al.*, 2011). Numerous studies have demonstrated strong relationships between glacial dynamic, oceanic circulation and sedimentary processes in the bay (Aksu, 1985, 1987; de Vernal *et al.*, 1987; Andrews *et al.*, 1998, 2014; Jennings *et al.*, 2014; Simon *et al.*, 2014; Nuttin and Hillaire-Marcel, 2015). Sedimentation occurs through two main processes: (1) glacial plumes from lateral sources with large volumes of fine-grained feldspar-rich sediments, which were transported to the area by sediment-laden supraglacial and subglacial meltwater or nepheloid layers and (2) Trans-Baffin icebergs drifting from the northern end of the bay with large volumes of coarse-grained carbonated sediments, leading to the deposition of so-called Baffin Bay Detrital Carbonate layers (BBDC; Simon *et al.*, 2014).

3. Material and methods

3.1. Core description

Core HU2008-029-016PC (70°46.14 N/-64°65.77 W; PC16 hereinafter) was raised from a 2063 m water depth, on the abyssal plain from central Baffin Bay. The 741-cm long core was retrieved using a piston corer during the 2008-029 CCGS Hudson cruise (Campbell and de Vernal, 2009). The sediment sequence is mainly composed of a succession of homogeneous dark gray to olive-gray silty clayey units and of very poorly sorted grayish-brown gravelly and sandy carbonate-rich layers (dolomite rich, Figure 2). These two lithofacies reflect the origin, transport and mode of deposition of the lithogenic sediments related to the ice sheet dynamics evoked above. Moreover, the top of the core down to 20 cm is characterized by brown to dark brown silty muds while the interval between 120 and 215 cm is constituted by brownish-black to olive-black clayey muds. These two distinct lithofacies represent sediments deposited respectively during the Holocene and during marine isotope stage (MIS) 2 (see Simon *et al.*, 2012, 2014, in prep. and Simon, 2013 for additional information).

3.2. Paleomagnetic results and chronology

The relative paleointensity (RPI) record previously established by a detailed paleomagnetic analysis (Simon *et al.*, 2012) reinforced and completed preliminary paleomagnetic results obtained on a shorter core from the same site (Thouveny 1988). The RPI proxy (Figure 2) is based on the normalization of the Natural Remanent Magnetization (NRM) with the Anhysteretic Remanent Magnetization (ARM) over the 25-35 mT AF demagnetization interval ($NRM_{25\text{-}35mT}$ /$ARM_{25\text{-}35mT}$). With the exception of few problematic layers, the ARM normalizer activates the same magnetic assemblages than the NRM, and the RPI proxy presents no correlation with lithological proxies. Moreover, the derived RPI record was favorably correlated with RPI reference curves and stacks in order to establish the initial chronology of the core (Simon *et al.*, 2012). These reference records included mainly the

North Atlantic relative paleointensity stack NAPIS-75 (Laj *et al.*, 2000) and the Labrador Sea core MD95-2024 (Stoner *et al.*, 2000). Two large inclination variations coeval with paleointensity lows allowing the recognition of two major geomagnetic excursions, *i.e.*, the Laschamp and Norwegian-Greenland-Sea excursions, and three-radiocarbon ages further supported the age model (see Simon *et al.*, 2012 for details). This initial chronology is considered robust for the MIS 2-3-4 periods with a high correlation between PC16 and the NAPIS-75 stack (r=0.82 between 22-75 ka, Figure 2) and remains unchanged in this study. For the lower part of the core, large chronological uncertainties (correlation coefficients with reference records <0.51) required revision in order to improve its resolution and to compare ^{10}Be production rate variations with references. Therefore, the chronology of core PC16 was updated by tuning the PC16 RPI curve with the ODP 1063 RPI record (Channel *et al.*, 2012) using 13 tie points (r=0.70 between 75-136 ka, Figure 2). The age model for ODP Site 1063 was constructed by tandem correlation of oxygen isotope and RPI data to calibrated reference templates using the Match protocol (Lisiecki and Lisiecki, 2002), improving its reliability. The revised age model offers a significantly improved statistical robustness and places the PC16 core bottom (741 cm) in the MIS 6 interval representing a 20 ka age shift from the Simon *et al.* (2012) age model. Using this refined age model, the average sedimentation rate for the sedimentary sequence is 5.4 cm/ka and presents large variability mainly related to glacial/deglacial history. The mean sedimentation rates during the Holocene (0-10.6 ka), Deglacial-peak (10.7-12 ka) and last Glacial (12.1-136.7 ka) periods are 1.9 cm/ka, 25.8 cm/ka and 5.5 cm/ka, respectively (Figure 8).

3.3. Sample preparation

Based on the paleomagnetic record and on U and Th-series isotope records, 76 subsamples of ~1 g (dry sediment) were collected along core PC16 and processed for the Be isotope analysis at the CEREGE National Cosmogenic Nuclides Laboratory (France) according to the

chemical procedure set-up by Bourlès *et al.* (1989) and summarized in Carcaillet *et al.* (2003, 2004a, 2004b) and Ménabréaz *et al.* (2011, 2012, 2014). The method is detailed here since the separation procedure has been modified prior to the AMS measurements. ^{10}Be and its stable isotope ^{9}Be were co-extracted from the authigenic phase of the sediments using 20 ml.g^{-1} sediment of 0.04 M hydroxylamine (NH_2OH-HCl) in a 25% acetic acid leaching solution at 95 ± 5°C for 7 hrs. A 2 ml aliquot of the resulting leaching solution was sampled for the measurement of the natural ^{9}Be concentration. The remaining solution was spiked with 300 µl of a 9.8039.10^{-4} g.g^{-1} ^{9}Be-carrier before the chemical extraction in order to accurately determine ^{10}Be sample concentrations from the measured ^{10}Be/^{9}Be ratios. The Be-purification was realized by chromatography in two stages. Before each separation stages, the samples were evaporated and then dissolved in ultra-pure HCl. Be oxy-hydroxides were precipitated at pH 8.5 from the solution by adding NH_3. The precipitate was separated by centrifugation, dissolved in ultra-pure HCl and then loaded onto an exchange column. The iron (Fe) and manganese (Mn) were separated using a Dowex® 1x8 (100–200 mesh) anion-exchange resin. The resin was first rinsed with 20 ml MilliQ water and conditioned with 20 ml 10.2 M HCl. The sample was then loaded onto the column and the Be fraction was collected immediately using 20 ml 10.2 M HCl for elution. The next purification step was carried out on a Dowex® 50x8 (100–200 mesh) cation-exchange resin in order to separate the Bore (B) and Aluminum (Al). The resin was rinsed with 30 ml MilliQ water and then conditioned with 30 ml 1 M HCl. After sample loading onto the column, the B and Be were eluted successively within the first 40 ml and next 120 ml of 1 M HCl eluent while the Al remained trapped within the column. After the two separation stages, Be oxy-hydroxides were precipitated at pH 8.5 from the final solution by adding NH_3. The precipitate was separated by centrifugation, rinsed by re-suspension using pH 8.5 buffered MilliQ water and centrifugated again. The purified Be oxy-hydroxides were solubilized in HNO_3 and the resulting solution was transferred into a quartz

crucible where it was gently evaporated to dryness at 200°C. Finally, the Be oxy-hydroxides deposit was oxidized and converted to BeO by heating at 800°C for 1 hr. The BeO was then mixed with Nb powder and pressed into a cleaned Ti cathode-holder in order to condition the samples for AMS measurements. In addition to sample processing, several routine blanks and 2 replicates were measured in order to assess both cleanliness and reproducibility during the chemical extraction.

3.4. Measurements

The natural authigenic ^{9}Be concentrations were measured using a graphite-furnace Atomic Absorption Spectrophotometer (AAS) with a double beam correction (Thermo Scientific ICE 3400®). The standard-addition method and the addition of a constant volume of $MgNO_3$ solution (matrix modifier) were used to eliminate the matrix effects during the absorption and to allow measurements near the detection limit. ^{9}Be sample concentrations (Table 1) were determined from repeated absorbance measurements (4 times) performed on each of the four 100 µl aliquots of the sample solution, three of them being spiked with increasing amount of a Sharlau ^{9}Be-carrier diluted to a known concentration ($0.27 - 0.34 \times 10^{-8}$ $g.g^{-1}$) using HNO_3 0.2%. The standard deviation of repeated absorbance measurements for each sample must be less than 3% to be accepted. After correcting for sample dilution, the authigenic ^{9}Be sample concentrations along core PC16 vary around $1.99 \pm 0.83.10^{-7}$ $g.g^{-1}$. The associated uncertainties (2σ) varying from 0.4 to 3.2% (average value: 1.5%) are based on the reproducibility of measurements and the least-square fitting between measured absorbance at each stages of the standard-addition method ($r^2 > 0.9995$).

The natural authigenic ^{10}Be concentration measurements were performed at the French AMS national facility ASTER (CEREGE). ^{10}Be sample concentrations are calculated from the measured spiked $^{10}Be/^{9}Be$ ratios normalized to the NIST 4325 Standard Reference Material

(2.79±0.03 x 10^{-11}; Nishiizumi *et al.*, 2007), and are decay-corrected using the ^{10}Be half-life ($T_{1/2}$) of 1.387 ± 0.012 Ma (Chmeleff *et al.*, 2010; Korschinek *et al.*, 2010):

$$Authigenic\left[{}^{10}Be\right]_{at}^{decay\cdot corrected} = \left(\frac{{}^{10}Be}{{}^{9}Be}\right)_{M} \times \left(\left[{}^{9}Be\right]_{at} + m_{spike} \times \left[{}^{9}Be\right]_{spike} \times \frac{N_A}{M^{9}Be}\right) \times e^{\left(\frac{\ln(2)}{T_{1/2}} \times t\right)} \quad (1)$$

where: $(^{10}Be/^{9}Be)_M$ is the measured Be ratio; m_{spike} and $[^{9}Be]_{spike}$ are respectively the mass and the concentration of the added spike; N_A is the Avogadro constant ($6.02214.10^{23}$ mol^{-1}); $M^{9}Be$ is the beryllium Molar Mass (9.0121822 $g.mol^{-1}$) and t is the time. The ^{9}Be concentrations measured at the AAS are transformed in atoms as follow:

$$Authigenic\left[{}^{9}Be\right]_{at} = \left[{}^{9}Be\right]_{AAS} \times m'_{sample} \times \frac{N_A}{M^{9}Be} \quad (2)$$

where: $[^{9}Be]_{AAS}$ is the concentration of natural authigenic ^{9}Be measured at the AAS and $m'_{sample} = m_{sample} \times \left(\frac{m_{leached} - m_{aliquot}}{m_{leached}}\right)$ is the weight of sediment remaining after aliquot sampling.

The uncertainties (2σ) in the measured ^{10}Be/^{9}Be ratios and in the calculated ^{10}Be concentrations result from statistical and instrumental error propagation (Arnold *et al.*, 2010) and vary from 1.3 to 3.7% (average value: 2.2%).

The authigenic natural ^{10}Be/^{9}Be ratios are derived using equations (1) and (2):

$$Authigenic\left(\frac{{}^{10}Be}{{}^{9}Be}\right) = \frac{\left[{}^{10}Be\right]_{at}^{decay\cdot corrected}}{\left[{}^{9}Be\right]_{at}} \quad (3)$$

The measured and calculated ratios and their uncertainties are presented in Table 1. The uncertainties (2σ) of the calculated authigenic ^{10}Be/^{9}Be ratios are derived from the propagation of both uncertainties and vary between 2.9 and 9% (average value: 5.5%). Chemistry blank ratios range from 5.3 × 10^{-15} to 1.5 × 10^{-14}, which is at least 3 orders of magnitude lower than the sample ^{10}Be/^{9}Be ratios.

3.5. Measurements of $^{230}Th_{xs}$ in Baffin Bay sediments

In this study, we benefit from recent U and Th-series isotope results from PC16 in order to calculate ^{10}Be-fluxes ($^{230}Th_{xs}$-normalized). The measurements and calculation used for determining $^{230}Th_{xs}$ are detailed in Nuttin and Hillaire-Marcel (2015). The estimated initial $^{230}Th_{xs}$ activities, recalculated in respect to the revised chronology, are extremely variable ranging from 0.118±0.081 to 5.293±0.212 dpm.g^{-1} (1.145 dpm.g^{-1} on average with a standard deviation of 0.977). Except for few samples, large surplus of $^{230}Th_{xs}$ above the production from dissolved-U decay in the overlying water column points toward a sediment-focusing environment related to ice margin dynamics during the last glacial period. The preserved, decay-corrected, $^{230}Th_{xs}$-normalized ^{10}Be deposition rates (referred to ^{10}Be-fluxes hereinafter) are calculated as follow:

$$Flux\left[{}^{10}Be\right] = \frac{\left[{}^{10}Be\right]_{at/g}^{decay.corrected} \times Z \times \beta_{230}}{{}^{0}A_{Th-230}^{xs}} \quad (4)$$

where: $[^{10}Be]^{decay.corrected}$ is the ^{10}Be concentration at the time of deposition in atoms per gram of sediment; Z is the water depth (2063 m); β_{230} is the ^{230}Th production rate from the seawater ^{234}U decays throughout the water column (2.67.10^{-2} dpm.m^{-3}.y^{-1}; François *et al.*, 2004) and ${}^{0}A_{Th-230}^{xs} = A_{Th-230}^{xs} \times e^{\left(\frac{\ln(2)}{T_{1/2}} \times t\right)}$ is the scavenged $^{230}Th_{xs}$ concentration at the time of deposition. The uncertainties (2σ) of the calculated ^{10}Be-fluxes are derived from the propagation of both uncertainties and vary between 1.6 and 25.1% (average value: 5.0%). Note that solely 2 samples have uncertainties above 10% representing probable measurement outliers. The water depth was considered constant in first approximation for the calculation. The Th analyses have been performed after total digestion of 1 g of sediment, while Be isotopes were extracted from 1 g of sediment after partial leaching (in order to avoid the extraction of matricial Be; Bourlès *et al.*, 1989). Given the difference of these two approaches, the ^{10}Be-fluxes calculated here thus represent minimal values. This should be considered when comparing our results

against reference values, but it does not prevent any qualitative interpretations. A constant leaching efficiency of ~60 % (Bourlès *et al.*, 1989) has been verified based on the results from Ménabréaz *et al.* (2011) and Ménabréaz (2012) and can be use for calibration.

4. Results and discussion

Sample concentrations, ratios and fluxes are listed in Table 1 and presented *vs.* depth along the core photos, CT-Scan images and description in Figures 3 and 5. Sample ratios and fluxes are presented *vs.* age in Figures 7 and 8. Note that all results and statistical averages are reported hereafter with a $\pm 2\sigma$ uncertainty.

4.1. Authigenic ^{10}Be and ^{9}Be concentrations

The authigenic ^{10}Be (decay-corrected) concentrations vary from 0.051±0.002 to 6.403±0.085 x 10^{8} at.g^{-1} (mean: 1.64 10^{8} at.g^{-1}; σ=1.74). Such broad variability (> 2 orders of magnitude) is unusual in marine records where ^{10}Be concentrations usually vary by factors of 2 or 3. Comparable large amplitude variation was only found in few polar cores from the Lomonosov Ridge (central Arctic), Fram Strait and the Ross Sea (Antarctica) where ^{10}Be concentration ranging from 0.2 to 19.5 x 10^{8} at.g^{-1} (Eisenhauer *et al.*, 1994; Spielhagen *et al.*, 1997, 2004; Aldahan *et al.*, 1997; Sjunneskog *et al.*, 2007) were interpreted as paleoclimatic signals with high (resp. low) ^{10}Be concentrations during Interglacial or major Interstadial (resp. Glacial) periods. Given the temporal resolution of core PC16, we can argue that in Baffin Bay the ^{10}Be concentration varies on shorter time scales and is not directly related to Glacial/Interglacial cycles contrary to the mechanism proposed for the Arctic Ocean. The mean ^{10}Be concentrations in Baffin Bay are slightly lower than values from the central Arctic and Arctic/Nordic Seas of 3-4 x 10^{8} at.g^{-1} and 6.7 x 10^{8} at.g^{-1}, respectively (Frank *et al.*, 2008; Eisenhauer *et al.*, 1994; Aldahan *et al.*, 1997), as well as with values from lower latitude sites such as the Portuguese margin and the Golf of Papua: ~4.4 x 10^{8} at.g^{-1} and ~5.6 x 10^{8} at.g^{-1},

293 respectively (Carcaillet *et al.*, 2004b; Ménabréaz *et al.*, 2011, 2014). A strict interpretation of
294 the ^{10}Be concentration in term of atmospheric fluxes between distinct sites must be avoided
295 because of environmental parameters. However, the overall low ^{10}Be concentration from
296 Baffin Bay compared to low-latitude and Arctic sites suggests relatively reduced ^{10}Be inputs
297 to the coring site (especially within the very low ^{10}Be concentration interval at 232-275 cm
298 depth).
299 The authigenic ^{9}Be concentrations vary from 0.621±0.004 to 3.269±0.065 x 10^{16} at.g^{-1} (mean:
300 1.33 10^{16} at.g^{-1}; σ=0.56). The variability of ^{9}Be concentration is about 25 times lower than the
301 ^{10}Be variation. Still, this range of variation (~5 times) is larger than the variability observed in
302 lower-latitude marine cores (~2 times), advocating for important ^{9}Be transport and deposition
303 changes along core PC16. The mean ^{9}Be concentration values from PC16 are lower than
304 those from the Portuguese margin and the Golf of Papua, 2-4 x 10^{16} at.g^{-1}, but slightly higher
305 than values from the central Arctic (0.6-1 x 10^{16} at.g^{-1}) and from ODP983 site (~0.25 x 10^{16}
306 at.g^{-1}; Knudsen *et al.*, 2008). Notwithstanding specific interpretations related to each sites,
307 this comparison reveals the strong association between ^{9}Be concentration and terrigenous
308 inputs (*e.g.*, Bourlès *et al.*, 1989; Brown *et al.*, 1992). We can argue that the central and
309 deepest part of Baffin Bay is a sediment-focusing area that received slightly more ^{9}Be inputs
310 than deep open ocean basins because of its proximity to continental margins and the reduced
311 size and shape of the bay. This is in accordance with the U-Th results from PC16 (Nuttin and
312 Hillaire-Marcel, 2015).
313 The fluctuations of ^{10}Be and ^{9}Be concentrations present a high correlation coefficient (r=0.88,
314 Table 2), suggesting that sources of ^{10}Be and ^{9}Be into the bay (Figure 3) are both located on
315 the boarding continents and that the atmospheric ^{10}Be component directly precipitated over
316 the bay likely represents minor amounts compared to these large inputs of continental origin.

4.2. Authigenic $^{10}Be/^{9}Be$ ratios

The authigenic $^{10}Be/^{9}Be$ ratios ranging from 0.043±0.003 to 2.624±0.123 x 10^{-8} (mean: 1.01 x 10^{-8}; σ=0.86) disclose a variability over almost 2 orders of magnitude very similar to those of ^{10}Be and ^{9}Be concentrations. The fact that authigenic $^{10}Be/^{9}Be$ ratio values are broadly coherent with $^{10}Be/^{9}Be$ ratio values ranging from 0.36 to 1.54 x 10^{-8} measured in Arctic rivers (Franck *et al.*, 2009) supports the continental origin of the dissolved beryllium in Baffin Bay. Measurements from the Baffin Bay watersheds are however required to further discuss this issue. The authigenic $^{10}Be/^{9}Be$ ratio population can be divided in two groups: values (1) lower than 10^{-8} and (2) higher than 10^{-8} (Table 1, Figures 3, 5 and 6). The first group has ^{10}Be concentrations and $^{10}Be/^{9}Be$ ratios similar to those found within poorly sorted diamicton layers of the Ross Ice Shelf (Sjunneskig *et al.*, 2007) and of Arctic sediments of the last 350 kyr (*e.g.*, Aldahan *et al.*, 1997). They are thus coherent with other records from Polar Regions. The second group presents higher values in range with the lower limits of authigenic $^{10}Be/^{9}Be$ ratios from mid-to-low-latitude cores with similar sedimentation rates (Carcaillet *et al.*, 2004b; Ménabréaz *et al.*, 2014). This nearly bi-modal distribution of the authigenic beryllium concentrations and ratios presents a strong affinity with lithofacies changes (Figures 3 and 5).

4.3. Beryllium and sedimentological features

From the authigenic Be result variations presented above, questions arise about the nature of the forcing parameters. In order to understand the links with lithofacies changes, core PC16 offers a unique opportunity because of the numerous multi-proxy results available. The detailed sedimentological features of core PC16 have been largely presented and discussed elsewhere (see Simon *et al.*, 2012, 2014, in prep.; Simon, 2013; Nuttin and Hillaire-Marcel, 2015 for details) and are beyond the scope of this paper. Sediment compositional variability in core PC16 is a combination of changes in sediment delivery, transport and provenance

directly related to ice margin dynamics (Simon *et al.*, 2014). This variability is illustrated here by grain-size (bulk and magnetic), density (CT number), XRF Ca/Fe and XRD Carbonate percents along with the images and CT-Scans of core PC16 (Figures 3 and 8) and summarized by a principal component analysis (PCA; Table S1, Figure 4) that disentangle the main compositional (mineralogy and grain-size) changes. The first principal component (PC1) accounts for 61% of the total variance and has positive loadings with proxies of coarse detrital carbonate layers such as dolomite and calcite (XRD), XRF Ca, density and >63 μm %; and negative loadings with proxies related to finer sediments, feldspars (XRD) and XRF Fe and Ti (Figures 3 and 4; Table 2). It highlights the two main sedimentation features from Baffin Bay: *i.e.*, coarse-grained carbonate-rich sediments transported by icebergs and sea ice originating from the northern end of the bay against fine-feldspar rich sediments originating from Greenland and Baffin Island (Simon *et al.*, 2014).

Table 2 presents the correlation coefficients between Be isotopes and the sedimentological parameters. As suggested from Figures 3 and 7, the high correlation coefficients between PC1 and Be isotopes and ratios (>-0.8) express a strong association with sedimentological parameters. The authigenic beryllium values (^{10}Be, ^{9}Be and ^{10}Be/^{9}Be ratios) generally present significant increases at levels corresponding to fine grained feldspar-rich intervals associated with increases of clay minerals (30-50%; Simon *et al.*, 2014) while coarse carbonate-rich sediments (30-40% dolomite and 10-15% calcite) are characterized by lower Be values (Figure 3). This pattern is consistent with the scavenging efficiency of dissolved Be that depends on the composition and size of the particles available in the water column. The authigenic beryllium (^{10}Be, ^{9}Be and ^{10}Be/^{9}Be ratios) and thorium-excess ($^{230}Th_{xs}$) distribution are strongly grain size dependent, with significant positive correlations with very fine to fine silts (2-8 μm) while clays (0-2 μm) and medium to very coarse silts (8-63 μm) does not present any significant correlations (Table 2). The high correlation of authigenic Be isotopes

with the 2-8 μm fraction rather than with the clay-sized material is intriguing because we expected larger association with the smaller particles (because of their higher specific surface area available). We tentatively explain these results by the cohesive behavior of the clay-sized material that tends to form aggregate. These aggregates would have faster sinking rates and lower specific surface area available for the adsorption of dissolve Be explaining higher scavenging rates associated with very fine to fine silts. To the opposite, the authigenic Be concentrations and ratios are significantly anti-correlated with the coarser intervals (>63 μm, Figure 3) related to iceberg transported sediments (*i.e.*, BBDC). Despite an overall similar behavior of both isotopes in respect to sedimentary parameters, the authigenic ^{10}Be concentrations and authigenic ^{10}Be/^{9}Be ratios are usually slightly more correlated with sedimentological parameters than ^{9}Be isotopes. We interpret this difference by distinct sources and transport processes between both isotopes. The continental inherited-^{10}Be (*i.e.*, atmospheric ^{10}Be deposited onto ice-sheets) are derived from the melting and calving of ice sheets and are released in the water column during the ice melting, while the ^{9}Be isotopes are mainly coming from the mechanical erosion of bedrocks at the basal interface of ice streams. It is likely that a fraction of the dissolved ^{9}Be isotopes was scavenged rapidly on the continental margins within the buoyant turbid meltwater plumes or nepheloid layers (*i.e.*, re-suspension of fine sediment particles by bottom currents) due to higher particles concentration (Bacon and Rutgers van der Loeff, 1989) while the ^{10}Be transported within icebergs or sea ice was exported farther from the sources. A fraction of ^{9}Be would thus be immobilized in glacial/river estuaries (Kusakabe *et al.*, 1991) and removed from the water column within the less saline meltwater plumes on the inner-shelf (Frank *et al.*, 2009; Ó Cofaigh *et al.*, 2013) rather than being transported to the centre of the bay. Therefore, despite complex relationships between granulomery and mineralogy of these sediments, we can claim

391 that the authigenic ^{10}Be signatures in Baffin Bay reveal local marine and glacial influences
392 from the surrounding continents instead of reflecting a global ^{10}Be-production signal.

393 4.4. ^{10}Be-fluxes ($^{230}Th_{xs}$-normalized)

394 The preserved vertical ^{10}Be deposition rates (^{10}Be-fluxes) varies from 0.717±0.046 to
395 25.388±0.973 x 10^8 at.cm^{-2}.ka^{-1} with a mean value of 6.94 x 10^8 at.cm^{-2}.ka^{-1} and a standard
396 deviation of 7.037 expressing a large variability (Table 1, Figure 5). When increased by a
397 factor of 40%, to encompass the methodological bias induced by the partial leaching of Be
398 isotopes *vs.* the total digestion of Th (see section 3.5), the ^{10}Be-fluxes are oscillating between
399 1.004±0.065 to 35.544±1.362 x 10^8 at.cm^{-2}.ka^{-1} with an average of 9.72 x 10^8 at.cm^{-2}.ka^{-1}
400 (Table 3). The Holocene average ^{10}Be-flux is estimated at 7.6±0.2 x 10^8 at.cm^{-2}.ka^{-1} (10.7±0.2
401 x 10^8 at.cm^{-2}.ka^{-1} value corrected), while during the glacial period the fluxes oscillated around
402 14.3±0.5 (20.1±0.7) and 2.0±0.2 (2.8±0.2) x 10^8 at.cm^{-2}.ka^{-1} within the carbonate-free and
403 carbonate-rich layers, respectively (carbonate layers are highlighted by white banding in
404 Figures 3 and 5). The Holocene ^{10}Be-fluxes are similar with the actual ^{10}Be production of
405 12.1±0.3 x 10^8 at.cm^{-2}.ka^{-1} (Monaghan *et al.*, 1986). During the glacial period, results of ^{10}Be-
406 fluxes ranging from 0.7 to 25.4 x 10^8 at.cm^{-2}.ka^{-1} are coherent with the bulk ^{10}Be-fluxes
407 calculated in the Arctic and Fram Strait that range from 2 x 10^8 to 33 x 10^8 at.cm^{-2}.ka^{-1}
408 (Eisenhauer *et al.*; 1994; Aldahan *et al.*, 1997). Despite an obvious sedimentological
409 relationship in core PC16, and at the exception of few intervals, the ^{10}Be-fluxes are
410 compatible with the modeled ^{10}Be-production range: ~3 to 27 x 10^8 at.cm^{-2}.ka^{-1}; with the
411 ^{10}Be-fluxes from ice and marine records which range from ~1.2 to 70 x 10^8 at.cm^{-2}.ka^{-1}, and
412 with the globally integrated and long-term averaged ^{10}Be-fluxes into marine sediments
413 varying between 9 to 28 × 10^8 at.cm^{-2}.ka^{-1} (see Table 3 for details and references). The lowest
414 ^{10}Be-fluxes that characterized the BBDC layers are also rather similar to those found within
415 the Ice Summit record of GISP2: 2 to 6 x 10^8 at.cm^{-2}.ka^{-1} (Muscheler *et al.*, 2004). It is

puzzling to obtain ^{10}Be-fluxes similar to ice core records in core PC16 given the strong lithogenic imprint. This similarity might be explained by a smoothing of the ^{10}Be cosmogenic nuclide signal related to the long-lasting deposition/drift onto the regional ice-sheets and by the thick sea ice and/or ice-shelf cover during glacial periods. The relatively low ^{10}Be-fluxes calculated in Baffin Bay would thus likely represent a ^{10}Be production signal buffered by the glacial factors controlling the ^{10}Be inputs and transport within the water column. Furthermore, these low ^{10}Be-fluxes from Baffin Bay are also coherent with the low depositions of ^{10}Be in Greenland and in the Arctic Ocean (Eisenhauer *et al.*, 1994; Spielhagen *et al.*, 1997) likely due to atmospheric circulation patterns and the distribution of precipitation in the northern hemisphere (Heikkila *et al.*, 2013; Frank *et al.*, 2009).

4.5. Testing the ^{10}Be/^{9}Be ratios and $^{230}Th_{xs}$-normalized ^{10}Be fluxes methods

The two existing normalization methods were independently used in former studies, but only two studies applied the two methods on the same sedimentary core. The first study by Knudsen *et al.* (2008) obtained large uncertainties about $^{230}Th_{xs}$ values precluding their use for reliable normalization. The second study by Ménabréaz *et al.* (2011) demonstrated close agreement of the results obtained by the two methods based on a small number of samples. In PC16, the ^{10}Be-flux variability calculated using the $^{230}Th_{xs}$ method is similar to that of the authigenic ^{10}Be/^{9}Be ratios measured at the same depths (Figure 5). The high correlation coefficient (r=0.81) and coherence between the two signals provide strong evidence that the two normalization processes yield equivalent results in a very contrasted environment where large compositional variations prevailed (Figures 5 and 6, Table 2). It somehow demonstrates that normalizing authigenic ^{10}Be concentrations by authigenic ^{9}Be concentrations permits an accurate correction for the total particle flux variation. Both normalization processes present large variations directly related to lithofacies changes (Figure 3). The normalizers (*i.e.*, $^{230}Th_{xs}$ and ^{9}Be) are highly correlated (Table 2) which might seem surprising given the distinct

affinities (depending on particle composition) and the different scavenging residence times of both elements in the open ocean (10-50 years for Th against 500-1000 years for Be, Chase *et al.*, 2002). The large domination of glaciomarine lithogenic particles presenting strong surface reactivity with both nuclides probably explained the first assertion (Roy-Barman *et al.*, 2005, 2009). Our results also suggest quicker adsorption rates and thus shorter scavenging residence time for dissolved Be within the Baffin Bay water column probably related to the high concentration of lithogenic particles. This is coherent with previous results from the Arctic, North Atlantic basin and circum-Antartica where lower scavenging residence time for Be isotopes of about 80-200 years associated with high particles concentration and oceanic mixing have been proposed (von Blanckenburg *et al.*, 1996, 1999; von Blanckenburg and Bouchez, 2014; Frank *et al.*, 2009). An oceanic circulation/mixing influence over the authigenic Be signal into Baffin Bay during the glacial period is also supported by higher correlation coefficients between both normalization methods when considering the rare episodes of Arctic Waters overflow through the Davis Strait (illustrated by blue dots in Figures 5 and 6). These episodes have been demonstrated within core PC16 by the occurrence of short periods of $^{230}Th_{xs}$ export ($^{230}Th_{xs}$-losses, Nuttin and Hillaire-Marcel, 2015).

4.6. Comparison with relative paleointensity

In core PC16, the comparison of ^{10}Be-proxies with the RPI record does not demonstrate any clear relationship (Figure 7). No systematic increases of authigenic $^{10}Be/^{9}Be$ ratios and ^{10}Be-fluxes are observed during the large RPI lows corresponding to the Laschamp, Norwegian-Greenland Sea and post-Blake/Blake events (Figure 7). The authigenic $^{10}Be/^{9}Be$ ratios and ^{10}Be-fluxes do not present any significant correlation coefficients with the RPI record (Figure 7, Table 2). This absence of correlation with the RPI record clearly supports the dominance of the environmental imprints –as discussed above- on the ^{10}Be deposition in Baffin Bay. The high correlation (r=0.83) between the RPI normalizers (such as the ARM) and the authigenic

466 $^{10}Be/^{9}Be$ ratios also indicates a strong environmental imprint related to specific grain-size
467 ranges that insure maximum Be adsorption rates (namely the very fine to fine silt range is
468 highly correlated with the ARM: r=0.7). The strong correlation of the ^{10}Be-proxies with
469 environmental parameters suggests a local signature related with the succession of events
470 driven by paleoclimatic controls precluding any interpretation of the ^{10}Be-proxies in term of
471 geomagnetic variability. On the opposite, our findings provide strong evidence supporting the
472 use of the cosmogenic nuclide ^{10}Be as a stratigraphic marker in the Arctic and sub-Arctic
473 regions as suggested by several authors (Eisenhauer *et al.*, 1994; Spielhagen *et al.*, 1997;
474 Aldahan *et al.*, 1997; Frank *et al.*, 2008).

475 **5. Paleoenvironmental implications**

476 The quasi bi-modal distribution of Be results in core PC16 corresponding with the main
477 Baffin Bay sedimentary features (Figure 3) and the temporal resolution of Be variations
478 suggest glacial dynamics as the main forcing parameter to explain Be inputs and transport
479 changes. The most striking features of this glacial dynamic around Baffin Bay is the
480 variability of the GIS limits over the Greenland continental shelf and the ice streaming events
481 from the LIS and IIS together with sea ice/ice-shelf cover variability (Figure 9). The origin,
482 timing and limits of these large glacial variations are still very poorly constrained. However,
483 recent studies have demonstrated that ice-sheets advanced well onto the continental margins
484 all over the bay and as far as the shelf edges during the LGM (Li *et al.*, 2011; Ó Cofaigh *et*
485 *al.*, 2012, 2013; Hogan *et al.*, 2012; Dowdeswell *et al.*, 2013; Simon *et al.*, 2014: Margold *et*
486 *al.*, 2015).

487 The cumulative inventory of measured $^{230}Th_{xs}$ in core PC16 (see Nuttin and Hillaire-Marcel,
488 2015 for details), recalculated in respect to the revised age model, clearly exhibits maximal
489 sediment fluxes corresponding to minimum relative sea level (RSL) during the LGM (Figure
490 8). High Be concentrations (Figures 7 and 8) and *ca.* 100% sediments originating from

491 Greenland (Simon *et al.*, 2014) also characterized this period. The other periods of high
492 authigenic Be concentrations are also associated with finer sediments originating mainly from
493 Greenland (Figure 8). This facies is related to the resuspension of fine lithogenic sediments
494 (glacial flour) associated to nepheloid layers during period of intense ice margin advances, to
495 outflow of dense winter water from the continental shelves, or to meltwater sediment-laden
496 plumes during period of ice margin retreats. Both scenarios imply ice margins/ice streams
497 extending over the Greenland continental shelf. Together with the inherent higher scavenging
498 efficiency of smaller particles, the increase in particle concentration due to the proximal ice
499 margin likely contributed to the increase of the Be-scavenging rates in central Baffin Bay
500 (Figure 9). We can also assume that a fraction of the Be transported onto ice floes sediments
501 might be transferred into the water column by wave wash-off or turning of floes during these
502 glacial maxima. Two ^{10}Be concentration values of 2.2±0.1 and 2.8±0.1 x 108 at.g^{-1} measured
503 in clay samples from Arctic ice floes (Eisenhauer *et al.*, 1994) and corresponding to the
504 higher ^{10}Be concentration values from PC16 support this assumption, although samples from
505 Baffin Bay are requested to further discuss this assertion.
506 On the other hand, the low authigenic Be concentrations and ratios within the BBDC layers
507 support a Be dilution in these IRD layers (Figure 2). Such a dilution is possibly associated to
508 (1) increases of terrigenous sediment inputs, (2) changes of sediment composition/grain-size
509 affecting the scavenging efficiency of dissolved beryllium, (3) reduced net Be inputs into the
510 centre of the bay and/or (4) higher exports of Be by extensive sea ice/iceberg drift episodes.
511 The absence of significant increases in sedimentation rates (Figure 8) and/or $^{230}Th_{xs}$ changes
512 (Nuttin and Hillaire-Marcel, 2015) during these intervals favor the last three hypotheses.
513 However one cannot totally exclude that short episodes of increased inputs of terrigenous
514 sediments could remain uncaptured by the age model resolution. During the BBDC intervals,
515 the limited amount of sediment originating from Greenland supports a distant Greenland ice

margin limit while coarse sediments originating from Baffin Island are explained by high calving rates from Laurentide ice streams (Simon *et al.*, 2014). According to this model, the BBDC intervals occur during periods of retreated ice limits over the inner continental shelves (Figure 9). The cause of ice margin instabilities around Baffin Bay is still not well understood but may be related to higher summer insolation and/or to the advection of warm Atlantic Water. Indeed the phasing between magnetic grain size in core PC16 ($SIRM/k_{LF}$ ratios in Figure 8, Simon *et al.*, 2012, 2014) and the insolation variation supports a climatic control on ice margin dynamics and iceberg drifting in the bay. The advection of an intermediate warm water mass in Baffin Bay probably contributed also to destabilize the ice margins (Holland et al., 2008; Jennings *et al.*, 2014) increasing meltwater delivery along the Baffin Bay shelves and slopes. It resulted in increased stratification of the water column and therefore to longer residence times of Be within the deep water masses (von Blanckenburg and O'Nions, 1999). Such an oceanic pattern would reduce the Be adsorption and deposition rates explaining possibly part of the low ^{10}Be concentration within the BBDC intervals. Moreover, and despite complex interactions of eustatic and isostatic parameters over the relative sea level (RSL) around Baffin Bay, we can reasonably assess that the sea level rose over continental shelves during ice margin retreat periods (Long et al., 2008; Simpson et al., 2009; Funder et al., 2011). Throughout these periods of marine transgression, oceanic circulation and boundary scavenging (changes in nature and intensity, Lao *et al.* 1992) may have become significant processes involving large transfer of dissolved Be from the centre of the bay toward the margins (Roy-Barman *et al.*, 2009). The low authigenic $^{10}Be/^{9}Be$ ratios and ^{10}Be-fluxes during the BBDC intervals within core PC16 might thus be partly explained by high boundary scavenging rates over the large Greenland continental shelf together with important iceberg/sea ice drifts due to very active Laurentide ice streams. For instance, the very low authigenic $^{10}Be/^{9}Be$ ratios found during the late MIS-3 (*ca.* 40-28.5 ka BP) is explained by

retreated GIS limits and numerous ice streaming episodes from the LIS and IIS possibly related to the Dansgaard-Oeschger events between the large glacial surges of Heinrich-events 3 and 4 (Figure 8; Simon et al., 2014).

Even though interpretations resulting from the authigenic Be signature in Baffin Bay can be discussed and are likely the results of several processes, we can reasonably proposed that the glacial dynamic of regional ice sheets (*i.e.*, GIS, IIS and LIS) is the main internal driving mechanism in term of ^{10}Be inputs and delivery into the bay. Moreover, ice-sheets topography changes related to such glacial dynamic also imply a reorganization of the atmospheric circulation (*e.g.*, Steffensen *et al.*, 2008) modifying the stratosphere/troposphere exchanges, the wet/dry deposition ratio and the dust inputs into the ocean (Werner *et al.*, 2002). Periods of ice-sheet growth (resp. decay) characterized by higher (resp. lower) wet deposition would then favor higher (resp. lower) ^{10}Be deposition rates within the bay. Although our results are coherent with these views, atmospheric modeling of ^{10}Be deposition considering regional ice-sheet topography changes are needed to verify and quantify these assumptions.

6. Conclusions

The authigenic ^{10}Be cosmogenic nuclide and ^{9}Be stable isotope data were measured along a 7.41 m sedimentary core of the sub-arctic basin Baffin Bay in order to reconstruct the geomagnetic dipole moment variations using the ^{10}Be/^{9}Be ratios and ^{10}Be-fluxes ($^{230}Th_{xs}$-normalized). The results of the two normalizations are coherent and reveal that environmental processes such as glacial dynamics and oceanic variability directly control the variations of the authigenic ^{10}Be and ^{9}Be concentrations in Baffin Bay sediments. The contribution of the atmospheric ^{10}Be cosmogenic nuclide production modulated by the geomagnetic field intensity remains hidden behind this environmental signal. Accordingly, in such conditions ^{10}Be production proxies do not allow to characterize the geomagnetic features such as dipole lows linked to excursions or reversals. Beryllium isotopes are preferentially adsorbed on fine

silicate particles associated with sediment plumes originating from lateral ice margin advances. On the contrary they have little affinity with coarse-grained and carbonate-rich sediments (*i.e.,* BBDC) associated with iceberg and sea-ice transport originated from the North-Eastearn Laurentide Ice Sheet and Innuitian Ice Sheet ice streaming events. During these BBDC episodes, glacial margin retreats together with marine transgression over the Greenland continental shelf likely contributed to increase boundary scavenging involving large transfers of dissolved beryllium from the centre of the bay toward the margins. Our findings provide strong evidences that support the use of cosmogenic nuclide ^{10}Be as a stratigraphic marker in the Arctic and sub-Arctic regions. Yet, our results caution a straightforward use of ^{10}Be-concentrations as a proxy of Interglacial/Glacial cycles or major Interstadial periods (as suggested by several authors), and rather propose to relate the ^{10}Be variations to higher-frequency paleoclimatic changes and glacial dynamics. Therefore, studying the cosmogenic ^{10}Be and stable ^{9}Be isotopes in combination with ancillary sedimentological parameters in arctic and sub-arctic marine sediments provide valuable climatic information, but is must be acknowledged that the cost/information ratio is probably too large to systematically use atmospheric ^{10}Be cosmogenic nuclides and ^{9}Be isotopes as paleoclimatic proxies.

Acknowledgements

We acknowledge Valery Guillou (CEREGE) for his help during chemical sample preparation and ^{9}Be measurements at the AAS. M. Arnold, G. Aumaître and K. Keddadouche are thanked for their valuable assistance during the measurements performed at the ASTER AMS national facility (CEREGE, Aix en Provence). This equipment is supported by the INSU/CNRS, the IRD and the CEAEA and by the ANR through the program "EQUIPEX Investissement d'Avenir". This study is a contribution of the project MAGORB ANR 09 BLAN 0053 (CEREGE, IPGP, LSCE). G. St-Onge and C. Hillaire-Marcel acknowledge financial support

from the Natural Science and Engineering Council of Canada (NSERC). CEREGE belongs to Observatoire des Sciences de l'Univers OSU-Institut Pythéas.

References

Aksu, A.E., 1985. Climatic and oceanographic changes over the past 400,000 years: evidence from deep-sea cores on Baffin Bay and Davis strait. In Quaternary Environments: Eastern Canadian Arctic, Baffin Bay and Western Greenland, Andrews JT (ed.). Allen and Unwin: Boston; 181–209.

Aksu, A.E., Piper, D.J.W., 1987. Late Quaternary Sedimentation in Baffin Bay. Canadian Journal of Earth Sciences 24 (9): 1833–46.

Aldahan, A.A., Ning, S., Possnert, G., Backman, J., Boström, K., 1997. ^{10}Be records from sediments of the Arctic Ocean covering the past 350 ka. Marine Geology 144 (1-3): 147-162.

Aldahan, A., Possnert, G., Johnsen, S., Clausen, H.B., Isaksson, E., Karlen, W., Hansson, M., 1998. Sixty year ^{10}Be record from Greenland and Antarctica. Proceedings of the Indian Academy of Sciences - Earth and Planetary Sciences 107 (2): 139–147.

Alexanderson, H., Backman, J., Cronin, T.M., Funder, S., Ingólfsson, Ó., Jakobsson, M., Landvik, J.Y., Löwemark , L., Mangerud, J., März, C., Möller, P., O'Regan, M., Spielhagen, R.F., 2014. An Arctic perspective on dating Mid-Late Pleistocene environmental history. Quaternary Science Reviews 92: 9-31.

Alley, R.B., Andrews, J.T., Brigham-Grette, J., Clarke, G.K.C., Cuffey, K.M., Fitzpatrick, J.J., Funder, S., Marshall, S.J., Miller, G.H., Mitrovica. J.X., 2010. History of the Greenland Ice Sheet: Paleoclimatic insights. Quaternary Science Reviews 29 (15–16): 1728-1756.

Andrews, J.T., Kirby, M.E., Aksu, A.E., Barber, D.C., Meese. D., 1998. Late Quaternary Detrital Carbonate (DC-) Layers in Baffin Bay Marine Sediments (67°–74° N): Correlation with Heinrich Events in the North Atlantic?. Quaternary Science Reviews 17: 1125-1137.

Andrews, J.T., Gibb, O.T., Jennings, A.E., Simon, Q., 2014. Variations in the provenance of sediment from ice sheets surrounding Baffin Bay during MIS 2 and 3 and export to the Labrador Shelf Sea: Site HU2008029-0008 Davis Strait. Journal of Quaternary Science 29 (1): 3-13, doi:10.1002/jqs.2643.

Arnold, M., Silke, M., Bourlès, D.L., Braucher, R., Benedetti, L., Finkel, R.C., Aumaître, G., Gottdang, A., Klein, M., 2010. The French accelerator mass spectrometry facility ASTER: Improved performance and developments. Nuclear Instruments and Methods in Physics Research B 268: 1954–1959, doi:10.1016/j.nimb.2010.02.107.

Auer, M., Wagenbach, D., Wild, E.M., Wallner, A., Priller, A., Miller, H., Schlosser, C., Kutschera, W., 2009. Cosmogenic ^{26}Al in the atmosphere and the prospect of a ^{26}Al/^{10}Be chronometer to date old ice. Earth and Planetary Science Letters 287: 453–462.

Bacon, M.P., 1984. Glacial to interglacial changes in carbonate and clay sedimentation in the Atlantic Ocean estimated from ^{230}Th measurements. Chemical Geology 46 (2): 97-111.

633 Bacon, M.P., Rutgers van der Loeff, M.M., 1989. Removal of thorium-234 by scavenging in
634 the bottom nepheloid layer of the ocean. Earth and Planetary Science Letters 92 (2):
635 157-164.

636 Barker, S., Knorr, G., Edwards, R.L., Parrenin, F., Putnam, A.E., Skinner, L.C., Wolff, E.,
637 Ziegler, M., 2011. 800,000 Years of Abrupt Climate Variability. Science 334 (6054):
638 347-351, doi:10.1126/science.1203580.

639 Baroni, M., Bard, E., Petit, J.R., Magand, O., Bourlès D.L., 2011. Volcanic and solar activity,
640 and atmospheric circulation influences on cosmogenic ^{10}Be fallout at Vostok and
641 Concordia (Antarctica) over the last 60 years. Geochimica et Cosmochimica Acta 75
642 (22): 7132-7145, doi:10.1016/j.gca.2011.09.002.

643 Beer, J, Blinov, A., Bonani, G., Finkel, R.C., Hofmann, H.J., Lehmann, B., Oeschger, H.,
644 Sigg, A., Schwander, J., Staffelbach, T., Stauffer, B., Sutter, M., Wötfli, W., 1990.
645 Use of ^{10}Be in Polar Ice to Trace the 11-Year Cycle of Solar Activity. Nature 347
646 (6289): 164–166, doi:10.1038/347164a0.

647 Beer, J., Finkel, R.C., Bonani, G., Gäggeler, H., Glach, U., Jacob, P., Klockow, D., Langway,
648 C.C.J., Neftel, A., Oeschger, H., Schotterer, U., Schwander, J., Siegenthaler, U., Suter,
649 M., Wagenbach, D., Wölfli, W., 1991. Seasonal variations in the concentrations of
650 ^{10}Be, Cl^-, NO^-_3, SO^{2-}_4, H_2O_2, ^{210}Pb, ^{3}H, mineral dust, and δ^{18}O in Greenland snow.
651 Atmospheric Environnemnt 25 (19): 899 – 904.

652 Bourlès, D.L., Raisbeck, G.M., Yiou, F., 1989. ^{10}Be and ^{9}Be in Marine sediments and their
653 potential for dating. Geochimica et Cosmochimica Acta 53 (2): 443–452.

654 Brown, E.T., Measures, C.I., Edmond, J.M., Bourlès, D.L., Raisbeck, G.M., Yiou, F., 1992.
655 Continental inputs of beryllium to the oceans. Earth and Planetary Science Letters 114
656 (1): 101-111.

657 Campbell D.C., de Vernal A., 2009. CCGS Hudson Expedition 2008029: Marine geology and
658 paleoceanography of Baffin Bay and adjacent areas, Nain, NL to Halifax, NS, August
659 28- September 23. Geological Survey of Canada, Open File 5989, 1 DVD.

660 Carcaillet, J.T., Thouveny, N., Bourlès, D.L., 2003. Geomagnetic moment instability between
661 0.6 and 1.3 Ma from cosmonuclide evidence. Geophysical Research Letters 30 (15):
662 1792, doi:10.1029/2003GL017550.

663 Carcaillet, J.T., Bourlès, D.L., Thouveny, N., 2004a. Geomagnetic dipole moment and ^{10}Be
664 production rate intercalibration from authigenic ^{10}Be/^{9}Be for the last 1.3 Ma.
665 Geochemistry Geophysics Geosystems 5 (5): Q05006, doi:10.1029/2003GC000641.

666 Carcaillet, J.T., Bourlès, D.L., Thouveny, N., Arnold, M. 2004b. A high resolution authigenic
667 ^{10}Be/^{9}Be record of geomagnetic moment variations over the last 300 ka from
668 sedimentary cores of the Portuguese margin. Earth and Planetary Science Letters 219
669 (3): 397–412, doi:10.1016/S0012821X03007027.

670 Cauquoin, A., 2013. Flux de ^{10}Be en Antarctique durant les 800,000 dernières années et
671 interpretation. PhD Thesis, Université Paris-Sud XI, pp. 206.

672 Cauquoin, A., Raisbeck, G.M., Jouzel, J., Bard, E., ASTER Team, 2014. No evidence for
673 planetary influence on solar activity 330,000 years ago. Astronomy and Astrophysics
674 561: A132, doi:10.1051/0004-6361/201322879.

675 Channell, J.E.T., Xuan, C., Hodell, D.A., 2009. Stacking paleointensity and oxygen isotope
676 data for the last 1.5 Myr (PISO-1500). Earth and Planetary Science Letters 283 (1-4):
677 14-23, doi:10.1016/j.epsl.2009.03.012.

678 Channell, J.E.T, Hodell, D.A., Curtis, J.H., 2012. ODP Site 1063 (Bermuda Rise) revisited:
679 oxygen isotopes, excursions and paleointensity in the Brunhes Chron. Geochemistry
680 Geophysics Geosystems 13 (1): Q02001, doi:10.1029/2011GC003897.

681 Chase, Z., Anderson, R.F., Fleisher, M.Q., Kubik, P.W., 2002. The influence of particle
682 composition and particle flux on scavenging of Th, Pa and Be in the ocean. Earth and
683 Planetary Science Letters 204 (1): 215-229.

684 Chmeleff, J., von Blanckenburg, F., Kossert, K., Jakob, D., 2010. Determination of the ^{10}Be
685 half-life by multicollector ICP-MS and liquid scintillation counting. Nuclear
686 instruments and methods in physics research B. 268 (2): 192-199,
687 doi:10.1016/j.nimb.2009.09.012.

688 Christl, M., Strobl, C., Mangini, A., 2003. Beryllium-10 in deep-sea sediments: a tracer for
689 the Earth's magnetic field intensity during the last 200,000 years. Quaternary Science
690 Reviews 22 (5-7): 725-739, doi:10.1016/S0277-3791(02)00195-6

691 Christl, M., Mangini, A. Kubik, P.W., 2007. Highly resolved beryllium-10 record from ODP
692 Site 1089 - a global signal?. Earth and Planetary Science Letters 257 (1-2): 245-258,
693 doi:10.1016/j.epsl.2007.02.035.

694 Christl, M., Lippold, J., Steinhilber, F., Bernsdorff, F., Mangini, A., 2010. Reconstruction of
695 global ^{10}Be production over the past 250 ka from highly accumulating Atlantic drift
696 sediments. Quaternary Science Reviews." Quaternary Science Reviews 29 (19-20):
697 2663-2672, doi:10.1016/j.quascirev.2010.06.017.

698 Cooke, D.J., Humble, J.E., Shea, M.A., Smart, D.F., Lund, N., Rasmussen, I.L, Byrnak, B.,
699 Goret, P., Petrou, N., 1991. On cosmic-ray cut-off terminology. Il Nuovo Cimento
700 14C (3): 213-234.

701 de Vernal, A., Hillaire-Marcel, C., Aksu, A.E., Mudie, P.J., 1987. Palynostratigraphy and
702 chronostratigraphy of Baffin Bay deep sea cores: climatostratigraphic implications.
703 Palaeogeography, Palaeoclimatology, Palaeoecology 61: 97-105.

704 Dowdeswell, J.A., Hogan, K.A., Ó Cofaigh, C., Fugelli, E.M.G., Evans, J., Noormets, R.,
705 2013. Late Quaternary ice flow in a West Greenland fjord and cross-shelf trough
706 system: submarine landforms from Rink Isbrae to Uummannaq shelf and slope.
707 Quaternary Science Reviews 92: 292-309, doi:10.1016/j.quascirev.2013.09.007.

708 Dunai, T.J., Lifton, N.A., 2014. The Nuts and Bolts of Cosmogenic Nuclide Production.
709 Elements 10 (5): 347-350. doi:10.2113/gselements.10.5.347.

710 Dyke, A.S., 2004. An outline of North American Deglaciation with emphasis on central and
711 Northern Canada. Developments in Quaternary Science 2: 373–424.

712 Eisenhauer, A., Spielhagen, R.F., Frank, M., Hentzschel, G., Mangini, A., Kubik, P.W.,
713 Dittrich-Hannen, B., Billen, T., 1994. ^{10}Be records of sediment cores from high
714 northern latitudes: Implications for environmental and climatic changes. Earth and
715 Planetary Science Letters 124 (1): 171-184.

716 England, J.H., Atkinson, N., Bednarski, J., Dyke, A.S., Hodgson, D.A., Ó Cofaigh, C., 2006.
717 The Innuitian Ice Sheet: configuration, dynamics and chronology. Quaternary Science
718 Reviews 25 (7-8): 689-703, doi:10.1016/j.quascirev.2005.08.007.

719 Finkel, R.C., Nishiizumi, K., 1997. Beryllium 10 concentrations in the Greenland Ice Sheet
720 Project 2 ice core from 3-40 ka, Journal of Geophysical Research 102 (C12): 26699-
721 26706, doi:10.1029/97JC01282.

722 Francois, R., Frank, M., van der Loeff, R., Michiel, M., Bacon, M.P., 2004. ^{230}Th
723 normalization: an essential tool for interpreting sedimentary fluxes during the late
724 Quaternary. Paleoceanography 19: PA1018, doi:doi:10.1029/2003PA000939.

725 Frank, M., Schwarz, B., Baumann, S., Kubik, P.W., Suter, M., Mangini, A., 1997. A 200 kyr
726 record of cosmogenic radionuclide production rate and geomagnetic field intensity
727 from ^{10}Be in globally stacked deep-sea sediments. Earth and Planetary Science Letters
728 149 (1-4): 121-129.

729 Frank, M., 2000. Comparison of cosmogenic radionuclide production and geomagnetic field
730 intensity over the last 200,000 years. Philosophical Transactions of the Royal Society
731 London A 358: 1089-1107, doi: 10.1098/rsta.2000.0575.

732 Frank, M., Backman, J., Jakobsson, M., Moran, K., O'Regan, M., King, J., Haley, B.A.,
733 Kubik, P.W., Garbe-Schönberg, D., 2008. Beryllium isotopes in central Arctic Ocean
734 sediments over the past 12.3 million years: stratigraphic and paleoclimatic
735 implications. Paleoceanography 23 (1): PA1S02, doi:10.1029/2007PA001478.

736 Frank, M., Porcelli, D., Andersson, P., Baskaran, M., Björk, G., Kubik, P.W., Hattendorf, B.,
737 Guenther, D., 2009. The dissolved beryllium isotope composition of the Arctic Ocean.
738 Geochimica et Cosmochimica Acta 73 (20): 6114–6133,
739 doi:10.1016/j.gca.2009.07.010.

740 Funder S., Kjellerup K.K., Kjær K.H., Ó Cofaigh, C., 2011. The Greenland Ice Sheet during
741 the past 300,000 Years: a review, In: Ehlers, J., Gibbard, P.L., Hughes, P.D., Editor(s),
742 Developments in Quaternary Sciences (15): 699-713.

743 Grant, K.M., Rohling, E.J., Bar-Matthews, M., Ayalon, A., Medina-Elizalde, M., Bronk
744 Ramsey, C., Satow, C., Roberts, A.P., 2012. Rapid coupling between ice volume and
745 polar temperature over the past 150,000 years. Nature 491: 744-747,
746 doi:10.1038/nature11593.

747 Heikkilä, U., Beer, J., Jouzel, J., Feichter, J., Kubik, P., 2008. ^{10}Be measured in a GRIP snow
748 pit and modeled using the ECHAM5-HAM general circulation model. Geophysical
749 Research Letters 35: L05817, doi:10.1029/2007GL033067

750 Heikkilä, U., Beer, J., Feichter, J., 2009. Meridional transport and deposition of atmospheric
751 ^{10}Be. Atmospheric Chemistry and Physics 9: 515–527.

752 Heikkilä, U., Beer, J., Abreu, J.A., Steinhilber, F., 2013. On the atmospheric transport and
753 deposition of the cosmogenic radionuclides (^{10}Be): a review. Space Science Reviews
754 176 (1-4): 321-332, doi:10.1007/s11214-011-9838-0.

755 Hemming, S.R., 2004. Heinrich events: massive late Pleistocene detritus layers of the North
756 Atlantic and their global climate imprint. Reviews of Geophysics 42 (1): RG1005,
757 doi:10.1029/2003RG000128.

758 Henken-Mellies, W.U., Beer, J., Heller, F., Hsü, K.J., Shen, C., Bonami, G., Hofmann, H.J.,
759 Suter, M., Wölfli, W., 1990. ^{10}Be and ^{9}Be in South Atlantic DSDP Site 519: relation
760 to geomagnetic reversals and to sediment composition. Earth and Planetary Science
761 Letters 98: 267-276.

762 Hillaire-Marcel, C., de Vernal, A., Aksu, A.E., Macko, S., 1989. High-resolution isotopic and
763 micropaleontological studies of upper Pleistocene sediment at ODP site 645, Baffin
764 Bay. Proceedings of the Ocean Drilling Program, Scientific Results 105: 599–616,
765 doi:10.2973/odp.proc.sr.105.138.1989.

766 Hogan, K.A., Dowdeswell, J.A., Ó Cofaigh, C., 2012. Glacimarine sedimentary processes and
767 depositional environments in an embayment fed by West Greenland ice streams.
768 Marine Geology 311-314:1-16, doi:10.1016/j.margeo.2012.04.006.

769 Holland, D.M., Thomas, R.H., de Young, B., Ribergaard, M.H., Lyberth, B., 2008.
770 Acceleration of Jakobshavn Isbrae triggered by warm subsurface ocean waters, Nature
771 Geoscience 1(10), 659-664.

772 Horiuchi, K., Uchida, T., Sakamoto, Y., Ohta, A., Matsuzaki, H., Shibata, Y., Motoyama, H.,
773 2008. Ice core record of ^{10}Be over the past millennium from Dome Fuji, Antarctica: a
774 new record of past solar activity and a powerful tool for stratigraphic dating.
775 Quaternary Geochronology 3, 253–261.

776 Jennings, A.E., Walton, M.E., Ó Cofaigh, C., Kilfeather, A.A., Andrews, J.T., Ortiz, J.D., de
777 Vernal, A., Dowdeswell, J.A., 2013. Paleoenvironments during Younger Dryas-Early
778 Holocene retreat of the Greenland Ice Sheet from outer Disko Trough, central west
779 Greenland. Journal of Quaternary Science 29 (1): 27-40, doi:10.1002/jqs.2652.

780 Klassen, R.A., Fisher, D.A., 1988. Basal-flow conditions at the northeastern margin of the
781 Laurentide Ice Sheet, Lancaster Sound. Canadian Journal of Earth Sciences 25 (11):
782 1740–1750.

783 Knudsen, M.F., Henderson, G.M., Frank, M., Mac Niocaill, C., Kubik, P.W., 2008. In-phase
784 anomalies in beryllium-10 production and palaeomagnetic field behaviour during the
785 Iceland Basin geomagnetic excursion. Earth and Planetary Science Letters 265 (3-4):
786 588-599, doi:10.1016/j.epsl.2007.10.051.

787 Korschinek, G., Bergmaier, A., Faestermann, T., Gerstmann, U.C., Knie, K., Rugel, G.,
788 Wallner, A., Dillmann, I., Dollinger, G., Lierse von Gostomski, Ch., Kossert, K.,
789 Maiti, M., Poutivtsev, M., Remmert, A., 2010. A new value for the half-life of ^{10}Be by
790 Heavy-Ion Elastic Recoil Detection and liquid scintillation counting. Nuclear
791 Instruments and Methods in Physics Research B. 268 (2): 187-191.
792 doi:10.1016/j.nimb.2009.09.020.

793 Kovaltsov, G.A., Usoskin, I.G., 2010. A new 3D numerical model of cosmogenic nuclide
794 ^{10}Be production in the atmosphere. Earth and Planetary Science Letters 291 (1-4):
795 182-188, doi:10.1016/j.epsl.2010.01.011.

796 Kusakabe, M., Ku, T.L., Southon, J.R., Liu, S., Vogel, J.S., Nelson, D.E., Nakaya, S.,
797 Cusimano, G.L., 1991. Be isotopes in rivers/estuaries and their oceanic budgets. Earth
798 and Planetary Science Letters 102 (3): 265-276.

799 Lal, D., Peters, B., 1967. Cosmic ray produced radioactivity on the Earth, in Handbuch der
800 Physik (Springer, New York), vol. XLVI/2: 551–612.

801 Lal, D., 1988. Theoretically expected variations in the terrestrial cosmic-ray production rates
802 of isotopes. In: Cini Castagnoli, G. (Ed.), Solar–Terrestrial Relationships and the
803 Earth Environment in the last Millennia. Soc. Italiana di Fisica, Bologna, pp. 216–233.

804 Laj, C., Kissel, C., Mazaud, A., Channell, J.E.T., Beer, J., 2000. North Atlantic
805 palaeointensity stack since 75 Ka (NAPIS-75) and the duration of the Laschamp
806 event. Philosophical Transactions of the Royal Society of London 358 (1768): 1009-
807 1025.

808 Lao, Y., Anderson, R.F., Broecker, W.S., 1992. Boundary scavenging and deep-sea sediment
809 dating: constraints from excess ^{230}Th and ^{231}Pa. Paleoceanography 7 (6): 783-798.

Laskar, J., Robutel, P., Joutel, F., Gastineau, M., Correia, A.C.M., Levrard, B., 2004. A long-term numerical solution for the insolation quantities of the Earth. Astronomy and Astrophysics 428 (1): 261–85, doi:10.1051/0004-6361:20041335.

Li, G., Piper, D.J.W., Campbell, D.C., 2011. The Quaternary Lancaster Sound trough-mouth fan, NW Baffin Bay. Journal of Quaternary Science 26 (5): 511-522, doi:10.1002/jqs.1479.

Lisiecki, L.E., Lisiecki, P.A., 2002. Application of dynamic programming to the correlation of paleoclimate records. Paleoceanography 17 (4): 1049, doi:10.1029/2001PA000733.

Long, A.J., Roberts, D.H., Simpson, M.J.R., Dawson, S., Milne, G.A., Huybrechts, P., 2008. Late Weichselian relative sea-level changes and ice sheet history in southeast Greenland. Earth and Planetary Science Letters 272 (1-2): 8–18, doi:10.1016/j.epsl.2008.03.042.Long, 2008.

MacLean, B., 1985. Geology of the Baffin Island Shelf, in Quaternary Environments: Eastern Canadian Arctic, Baffin Bay and Western Greenland, edited by J.T. Andrews, pp. 154–177, Allen and Unwin, Boston.

Marcott, S.A., Clark, P.U., Padman, L., Klinkhammer, G.P., Springer, S.R., Liu, Z., Otto-Bliesner, B.L., Carlson, A.E., Ungerer, A., Padman, J., 2011. Ice-shelf collapse from subsurface warming as a trigger for Heinrich events. Proceedings of the National Academy of Sciences 108 (33): 13415–13419, doi:10.1073/pnas.1104772108.

Margold, M., Stokes, C.R., Clark, C.D., 2015. Ice streams in the Laurentide Ice Sheet: Identification, characteristics and comparison to modern ice sheets. Earth Science Reviews 143: 117-146, doi:10.1016/j.earscirev.2015.01.011

Masarik, J., Beer, J. 1999. Simulation of particle fluxes and cosmogenic nuclide production in the Earth's atmosphere. Journal of Geophysical Research 104 (D10): 12099-12111.

Masarik, J., Beer, J. 2009. An updated simulation of particle fluxes and cosmogenic nuclide production in the Earth's atmosphere. Journal of Geophysical Research 114: D11103, doi:10.1029/2008JD010557.

Ménabréaz, L., Thouveny, N., Bourlès, D.L., Deschamps, P., Hamelin, B., Demory, F., 2011. The Laschamp geomagnetic dipole low expressed as a cosmogenic ^{10}Be atmospheric overproduction at ~41ka. Earth and Planetary Science Letters 312 (3-4): 305-317, doi:10.1016/j.epsl.2011.10.037.

Ménabréaz, L., Bourlès, D.L., Thouveny, N., 2012. Amplitude and timing of the Laschamp geomagnetic dipole low from the global atmospheric ^{10}Be overproduction: contribution of authigenic ^{10}Be/^{9}Be ratios in west equatorial Pacific sediments. Journal of Geophysical Research 117: B11101, doi:10.1029/2012JB009256.

Ménabréaz, L., 2012, Production atmosphérique du nucléide cosmogénique ^{10}Be et variations de l'intensité du champ magnétique terrestre au cours des derniers 800 000 ans. PhD Thesis, Aix-Marseille Université, pp. 292.

Ménabréaz, L., Thouveny, N., Bourlès, D.L., Vidal, L., 2014. The geomagnetic dipole moment variation between 250 and 800 ka BP reconstructed from the authigenic ^{10}Be/^{9}Be signature in West Equatorial Pacific sediments. Earth and Planetary Science Letters. Earth and Planetary Science Letters 385: 190-205, doi:10.1016/j.epsl.2013.10.037.

Monaghan, M.C., Krishnaswami, S., Turekian, K.K., 1986. The global-average production rate of ^{10}Be. Earth and Planetary Science Letters 76: 279–287.

Murayama, M., Nagai, H., Imamura, M., Hatori, S., Kobayashi, K., Taira, A., 1997. ^{10}Be and 9Be concentrations in the deep sea sediment at site 925, Ceara Rise, in the western equatorial Atlantic: implication of ^{10}Be flux change. Shackleton, N.J., Curry, W.B., Richter, C., and Bralower, T.J. (Eds.). Proceedings of the Ocean Drilling Program, Scientific Results, Vol. 154: 389-394.

Muscheler, R., Beer, J., Wagner, G., Laj, C., Kissel, C., Raisbeck, G.M., Yiou, F., Kubik, P.W., 2004. Changes in the carbon cycle during the last deglaciation as indicated by the Comparison of ^{10}Be and ^{14}C records. Earth and Planetary Science Letters 219: 325-340, doi:10.1016/S0012-821X(03)00722-2.

Muscheler, R., Beer, J., Kubik, P.W., Synal, H.A., 2005. Geomagnetic field intensity during the last 60,000 years based on ^{10}Be and ^{36}Cl from the Summit ice cores and ^{14}C. Quaternary Science Reviews 24 (16-17): 1849-1860, doi:10.1016/j.quascirev.2005.01.012.

Nishiizumi, K., Imamura, M., Caffee, M.W., Southon, J.R., Finkel, R.C., McAninch, J., 2007. Absolute calibration of ^{10}Be AMS standards. Nuclear Instruments and Methods in Physics Research Section B 258: 403–413.

Nuttin, L., Hillaire-Marcel, C., 2015. U- and Th-series isotopes in deep Baffin Bay sediments: Tracers of detrital sources and of contrasted glacial/interglacial sedimentary processes. Marine Geology 361: 1-10. doi:10.1016/j.margeo.2015.01.003.

Ó Cofaigh, C., Andrews, J.T., Jennings, A.E., Dowdeswell, J.A., Hogan, K.A., Kilfeather, A.A., Sheldon, C., 2012. Glacimarine lithofacies, provenance and depositional processes on a West Greenland trough-mouth fan. Journal of Quaternary Science 28 (1): 13-26, doi:10.1002/jqs.2569.

Ó Cofaigh, C., Dowdeswell, J.A., Jennings, A.E., Hogan, K.A., Kilfeather, A.A., Hiemstra, J.F., Noormets, R., Evans, J., McCarthy, D.J., Andrews, J.T., Lloyd, J.M., Moros, M., 2013. An extensive and dynamic ice sheet on the West Greenland shelf during the last glacial cycle. Geology 41 (2): 219-222, doi:10.1130/G33759.1.

O'Brien, K., 1979. Secular variations in the production of cosmogenic isotopes in the Earth's atmosphere. Journal of Geophysical Research 84: 423–431.

O'Brien, K., de La Zerda Lerner, A., Shea, M., Smart, D., 1991. The production of cosmogenic isotopes in the Earth's atmosphere and their inventories. In: Sonett, C.P., Giampapa, M.S., Matthews, M.S. (Eds.), The Sun in Time. The University of Arizona, pp. 317–342.

Pedro, J., Van Ommen, T.D., Curran, M.A.J., Morgan, V., Smith, A., Mc Morrow, A., 2006. Evidence for climate modulation of the ^{10}Be solar activity proxy. Journal of Geophysical Research 111: D21105, doi:10.1029/2005JD006764.

Raisbeck, G.M., Yiou, F., Fruneau, M., Loiseaux, J.M., Lieuvin, M., Ravel, J.C., 1981. Cosmogenic ^{10}Be/^{7}Be as a probe of atmospheric transport processes. Geophysical Research Letters 8 (9): 1015–1018, doi:10.1029/GL008i009p01015.

Raisbeck, G.M., Yiou, F., Bourlès, D., Kent, D.V., 1985. Evidence for an increase in cosmogenic ^{10}Be during a geomagnetic reversal. Nature 315, 315–317, doi:10.1038/315315a0.

Raisbeck, G.M., Yiou, F., Jouzel, J., Petit, J.R., Bard, E., Barkov, N.I., 1992. ^{10}Be deposition at Vostok, Antarctica, during the last 50000 years and its relationship to possible cosmogenic production variations during this period. In: Bard, E., Broecker, W.S.

(Eds.), The Last Deglaciation: Absolute and Radiocarbon Chronologies, Series I. Glob. Environmental Change 2, pp. 127–139.

Raisbeck, G.M., Yiou, F., Cattani, O., Jouzel, J., 2006. ^{10}Be evidence for the Matuyama–Brunhes geomagnetic reversal in the EPICA Dome C ice core. Nature 444 (7115): 82-84, doi:10.1038/nature05266.

Robinson, C., Raisbeck, G.M., Yiou, F., Lehman, B., Laj, C., 1995. The relationship between ^{10}Be and geomagnetic field strength records in central North Atlantic sediments during the last 80 ka. Earth and Planetary Science Letters 136 (3): 551-557, doi:10.1016/0012-821X(95)00202-N.

Roy-Barman, M., Jeandel, C., Souhaut, M., Rutgers van der Loeff, M., Voege, I., Leblond, N., Freydier, R., 2005. The influence of particle composition on thorium scavenging in the NE Atlantic ocean (POMME Experiment). Earth and Planetary Science Letters 240 (3): 681-693.

Roy-Barman, M., 2009. Modelling the effect of boundary scavenging on Thorium and Protactinium profiles in the ocean. Biogeosciences 6 (12): 3091–3107.

Sellén, E., Jakobsson, M., Frank, M., Kubik, P.W., 2009. Pleistocene variations of beryllium isotopes in central Arctic Ocean sediment cores. Global and Planetary Change 68: 38–47.

Simon, Q., St-Onge, G., Hillaire-Marcel, C., 2012. Late Quaternary chronostratigraphic framework of deep Baffin Bay glaciomarine sediments from high-resolution paleo-magnetic data. Geochemistry, Geophysics, Geosystems 13 (1-24): Q0AO03, doi:10.1029/2012GC004272.

Simon, Q., Hillaire-Marcel, C., St-Onge, G., Andrews, J.T., 2014. North-eastern Laurentide, western Greenland and southern Innuitian ice stream dynamics during the last glacial cycle. Journal of Quaternary Science 29 (1): 14-26, doi:10.1002/jqs.2648.

Simon Q. 2013. Propriétés magnétiques, minéralogiques et sédimentologique des sédiments profond de la baie de Baffin: chronologie et dynamique des glaciers ouest groenlandais, innuitiens et laurentidiens au cours de la dernière glaciation. PhD Thesis, Université du Québec à Montreal, pp. 181.

Simon Q, Hillaire-Marcel C, St-Onge G. (in prep). Detrital carbonate events in Baffin Bay during the last climatic cycle: Their timing vs. the Greenland Dansgaard-Oeschger cycles and North Atlantic Heinrich events.

Simpson, M.J.R., Milne, G.A., Huybrechts, P., Long, A.J., 2009. Calibrating a glaciological model of the Greenland Ice Sheet from the Last Glacial Maximum to present-day using field observations of relative sea level and ice extent. Quaternary Science Reviews 28 (17-18): 1631–57.

Sjunneskog, C., Scherer, R., Aldahan, A., Possnert, G., 2007. ^{10}Be in glacial marine sediment of the Ross Sea, Antarctica, a potential tracer of depositional environment and sediment chronology. Nuclear Instruments and Methods in Physics Research Section B 259 (1): 576-583, doi:10.1016/j.nimb.2007.01.203.

Spielhagen, R.F., Bonani, G., Eisenhauer, A., Frank, M., Frederichs, T., Kassens, H., Kubik, P.W., Mangini, A., Nøgaard Pedersen, N., Nowaczyk, N.R., Schäper, S., Stein, R., Thiede, J., Tiedemann, R., Washner, M., 1997. Arctic Ocean evidence for late Quaternary initiation of northern Eurasian ice sheets. Geology 25 (9): 783-786.

Steffensen, J.P., Andersen, K.K., Bigler, M., Clausen, H.B., Dahl-Jensen, D., Fischer, H., Goto-Azuma, K., Hansson, M., Johnsen, S.J., Jouzel, J., Masson-Delmotte, V., Popp, T., Rasmussen, S.O., Röthlisberger, R., Ruth, U., Stauffer, B., Siggaard-Andersen, M.L., Sveinbjörnsdóttir, A.E., Svensson, A., White, J.W.C., 2008. High-Resolution Greenland Ice Core Data Show Abrupt Climate Change Happens in Few Years. Science 321 (5889): 680-684, doi:10.1126/science.1157707.

Steig, E.J., Polissar, P.J., Stuiver, M., Grootes, P.M., Finkel, R.C., 1996. Large amplitude solar modulation cycles of ^{10}Be in Antarctica: Implications for atmospheric mixing processes and interpretation of the ice core record. Geophysical Research Letters 23 (5): 523–526.

Stoner, J.S., Channell, J.E.T., Hillaire-Marcel, C., Kissel, C., 2000. Geomagnetic paleointensity and environmental record from Labrador Sea core MD95-2024: global marine sediment and ice core chronostratigraphy for the last 110 kyr. Earth and Planetary Science Letters 183 (1-2): 161-177.

Thouveny, N., 1988. High-resolution palaeomagnetic study of late Pleistocene sediments from Baffin Bay: first results. Canadian Journal of Earth Sciences 25: 833-843.

Thouveny, N., Bourlès, D.L., Saracco, G., Carcaillet, J.T., Bassinot, F., 2008. Paleoclimatic context of geomagnetic dipole lows and excursions in the Brunhes, clue for an orbital influence on the geodynamo?. Earth and Planetary Science Letters 275 (3-4): 269-284, doi:10.1016/j.epsl.2008.08.020.

Valet, J.P., Bassinot, F., Bouilloux, A., Bourlès, D.L., Nomade, S., Guillou, V., Lopes, F., Thouveny, N., Dewilde, F., 2014. Geomagnetic, cosmogenic and climatic changes across the last geomagnetic reversal from Equatorial Indian Ocean sediments. Earth and Planetary Science Letters 397: 67-79, doi:10.1016/j.epsl.2014.03.053.

von Blanckenburg, F., O'Nions, R.K., Belshaw, N.S., Gibb, A., Hein, J.R., 1996. Global distribution of beryllium isotopes in deep ocean water as derived from Fe-Mn crusts. Earth and Planetary Science Letters 141 (1): 213–226.

von Blanckenburg, F., O'Nions, R.K., 1999. Response of beryllium and radiogenic isotope ratios in Northern Atlantic Deep Water to the onset of northern hemisphere glaciation. Earth and Planetary Science Letters 167 (3): 175-182.

von Blanckenburg, F., Bouchez, J., 2014. River fluxes to the sea from the ocean's 10Be/9Be ratio. Earth and Planetary Science Letters 387: 34–43.

Vogt, S., Herzog, G.F., Reedy, R.C., 1990. Cosmogenic nuclides in extraterrestrial materials. Reviews of Geophysics 28 (3): 253-275.

Wagner, G., Masarik, J., Beer, J., Baumgartner, S., Imboden, D., Kubik, P.W., Synal, H.A., Suter, M., 2000. Reconstruction of the geomagnetic field between 20 and 60 kyr BP from cosmogenic radionuclides in the GRIP ice core. Nuclear Instruments and Methods in Physics Research B 172: 597-604

Webber, W.R., Soutoul, A., Kish, J.C., Rockstroh, J.M., 2003. Updated formula for calculating partial cross sections for nuclear reactions of nuclei with $Z \leq 28$ and $E >$ 150 MeV nucleon-1 in hydrogen targets. The Astrophysical Journal Supplement Series 144: 153-167.

Webber, W.R., Higbie, P.R., McCracken, K.G., 2007. Production of the cosmogenic isotopes ^{3}H, ^{7}Be, ^{10}Be, and ^{36}Cl in the Earth's atmosphere by solar and galactic cosmic rays. Journal of Geophysical Research 112: A10106, doi:10.1029/2007JA012499.

Werner, M., Tegen, I., Harrison, S.P., Kohfeld, K.E., Prentice, I.C., Balkanski, Y., Rodhe, H., Roelandt, C., 2002. Seasonal and interannual variability of the mineral dust cycle under present and glacial climate conditions. Journal of Geophysical Research 107 (D24), 4744, doi:10.1029/2002JD002365.

Yiou, F., Raisbeck, G.M., Bourlès, D.L., Lorius, C., Barkov, N.I., 1985. ^{10}Be in ice at Vostok Antarctica during the last climatic cycle. Nature 316 (6029): 616-617.

Yiou, F., Raisbeck, G.M., Baumgartner, S., 1997. Beryllium 10 in the Greenland Ice Core Project ice core at Summit, Greenland. Journal of Geophysical Research 102 (C12): 26783-26794.

Table 1. AMS measurements, authigenic ^{10}Be and ^{9}Be concentrations, authigenic ^{10}Be/^{9}Be ratios and calculated ^{10}Be-fluxes of core HU2008-029-016PC samples.

Table 2. Correlation coefficients of Be isotopes (concentration, ratio and fluxes) and sedimentological parameters.

Table 3. ^{10}Be-production/flux in litterature (in atoms.cm^{-2}.kyr^{-1})

Figure 1. General bathymetry, simplified oceanic circulation, sketch of the Paleozoic outcrops (*MacLean*, 1985) and paleo-Ice-Sheets (including LGM unknown maximum ice margin extents) of the Baffin Bay region. The location of HU2008-029-016PC sampling site is indicate by a red dots. Red arrows illustrate Atlantic "warm" waters, whereas the blue arrows represent colder Arctic waters. The simplified representations of the Greenland (green), Innuitian (blue) and Laurentide ice sheet (red) limits and major ice stream locations during the LGM (colored areas) are adapted from *Funder et al.* (2011), *Dyke* (2004) and *England et al.* (2006).

Figure 2. Relative paleointensity (NRM/ARM$_{25\text{-}35mT}$) tuned on RPI record of ODP Site 1063 (Channell *et al.*, 2012) and chronostratigraphy of PC16. The RPI tie-points used in this study are represented by green dots while the red diamonds and yellow triangle are radiocarbon ages and calcite tie-points respectively (Simon *et al.*, 2012). The incertitude in the age model is represented by shaded area.

Figure 3. Beryllium isotopes results *vs.* high-resolution physical, geochemical and mineralogical results from core PC16. Log: general simplified stratigraphy of the core; CT: CAT-Scan image of the core; HRI: high-resolution digital image; CT Number (density proxy); XRD carbonates (dolomite and calcite) cumulative percents; log(Ca/Fe): μXRF element ratio for calcium and iron measured with the ITRAX© core scanner. Grain size (%) for clay, silt fractions and coarse fractions measured at 4 cm intervals by laser diffraction. Authigenic ^{10}Be, ^{9}Be and ^{10}Be/^{9}Be ratios are display in log scale. Distinct lithological facies

are highlighted with color banding. Red: uppermost brownish gray silty mud unit (Uppermost Brownish, "UB"); light green: olive-black silty to clayey mud unit (Olive Clay, "OC"); white: carbonate-rich yellowish-brown to dark- brown very poorly sorted gravelly sandy mud detrital layers (DC); dark green: olive gray to dark gray poorly sorted silty to sandy mud low carbonate detrital layers (LDC) (see text for details).

Figure 4. Principal component analysis (PCA) of the mineralogical and grain-size dataset. The loading scores for PC1 vs. PC2 explain, respectively, 61 and 11.5% of the total variance. PCA analysis illustrates the two sedimentary modes in Baffin Bay.

Figure 5. Authigenic $^{10}Be/^{9}Be$ ratios and ^{10}Be-fluxes on depth. The ^{10}Be-fluxes are compared to references: (1) global-average ^{10}Be-production values from models, see Table 3 for values and references (the blue star is the mean value from Masarik and Beer, 2009); (2) global values measured and averaged by Monaghan *et al.*, 1986; (3) ^{10}Be-flux in GRIP/GISP2 ice core (Muscheler *et al.*, 2005); (4) ^{10}Be-flux in marine records representing the so-called "allowed range" from Christl *et al.*, 2007, 2010; (5) ^{10}Be-flux range in deep sea sedimentary cores from the Arctic Ocean and the Norwegian Sea (Eisenhauer *et al.*, 1994). Red (resp. blue) dots represent measured $^{230}Th_{xs}$ vertical flux higher (resp. lower) than theoretical $^{230}Th_{xs}$ vertical flux.

Figure 6. Authigenic $^{10}Be/^{9}Be$ ratios *vs.* ^{10}Be-fluxes ($^{230}Th_{xs}$-normalized). Blue dots represent measured $^{230}Th_{xs}$-flux samples lower than theoretical flux and illustrate episodes of Arctic Waters outflow through Davis Strait (Nuttin and Hillaire-Marcel, 2015).

Figure 7. Authigenic $^{10}Be/^{9}Be$ ratios, ^{10}Be-fluxes ($^{230}Th_{xs}$-normalized), PC 1 and RPI *vs.* age. RPI (Channell *et al.*, 2012) and ^{10}Be-fluxes (Christl *et al.*, 2010) from ODP Site 1063 are presented along with ^{10}Be-fluxes reference ranges from distinct archives and models (see Figure 5 and Table 3 for references). Marine isotopic stages 1 to 6 are represented by color boxes along the age axis. BBDC-layers are represented by a vertical grey banding and numbered according to Simon *et al.* (in prep.).

Figure 8. Paleoclimatic interpretations of authigenic $^{10}Be/^{9}Be$ ratio variations. The NGRIP $\delta^{18}O$ ice core record (red curves) and synthetic Greenland record (GLT-syn, blue curve) are from www.icecores.dk and Barker *et al.* (2011). Marine isotope stages 1 to 6 are represented with color boxes. BBDC-layers (defined by high XRD carbonates cumulative percents) are represented by the grey vertical bars and numbered according to Simon *et al.*, (in prep.). The North Atlantic Heinrich events (*Hemming*, 2004) are indicated for comparison. The July insolation is calculated at 70°N (from *Laskar et al.*, 2004). Eustatic relative sea level (RSL) is from *Grant et al.* (2012). $SIRM/k_{LF}$ is a magnetic grain size proxy (Simon *et al.*, 2012, in

prep.). The cumulative inventory ratio compares the $^{230}Th_{xs}$ accumulation fluxes with the theoretical vertical production in the overlying water column. Values below 1 during the Holocene indicate $^{230}Th_{xs}$-losses while values above 1 during the glacial period suggest a sediment-focusing environment (Nuttin and Hillaire-Marcel, 2015).

Figure 9. Simplified Baffin Bay paleogeography during the last glacial cycle. (a) Trans-Baffin drift characterized by IRD sediments originating from the northern ice streams, and by meltwater sediment-laden plumes from Baffin Island ice streams. (b) Extended ice margins characterized by Greenland and Baffin Island glacial flour sediments corresponding to a permanently ice-covered bay, and by extended ice margin limits over continental shelves.

Table1

Table 1. AMS measurements, authigenic ^{10}Be and ^{9}Be concentrations, authigenic $^{10}Be/^{9}Be$ ratios and calculated ^{10}Be-fluxes of core HU2008-029-016PC samples.

Depth in core (cm)	Age Model 17/07/14B (ka cal BP)	Sample weight (g)	Measured $^{10}Be/^{9}Be$ (10^{-11})*	Authigenic decay corrected [^{10}Be] (10^{8} at/g)*	Authigenic [^{9}Be] (10^{16} at/g)*	Authigenic $^{10}Be/^{9}Be$ (10^{-8})*	Flux ^{10}Be Th_norm.[a] (10^{8} atoms.cm^{-2}kyr^{-1})
0.5	0.80	0.994	3.011 ± 0.040	6.403 ± 0.085	3.269 ± 0.065	1.959 ± 0.094	7.753 ± 0.131
8.5	4.85	0.963	1.976 ± 0.029	4.326 ± 0.064	3.060 ± 0.054	1.417 ± 0.065	8.571 ± 0.181
16.5	9.68	1.000	0.797 ± 0.013	1.687 ± 0.027	1.930 ± 0.029	0.878 ± 0.038	6.522 ± 0.157
24.5	10.83	1.000	0.144 ± 0.003	0.304 ± 0.007	1.229 ± 0.011	0.249 ± 0.012	2.021 ± 0.063
32.5	10.98	0.990	0.218 ± 0.006	0.468 ± 0.012	1.048 ± 0.007	0.449 ± 0.024	3.044 ± 0.107
40.5	11.41	0.983	0.060 ± 0.002	0.129 ± 0.004	0.898 ± 0.029	0.144 ± 0.013	0.837 ± 0.028
48.5	11.91	0.988	0.038 ± 0.001	0.081 ± 0.003	0.740 ± 0.013	0.110 ± 0.008	1.916 ± 0.174
56.5	12.13	0.961	0.089 ± 0.002	0.195 ± 0.005	1.028 ± 0.023	0.191 ± 0.013	3.756 ± 0.363
64.5	12.76	1.074	0.408 ± 0.008	0.801 ± 0.016	1.090 ± 0.009	0.740 ± 0.032	
72.5	13.39	0.932	0.526 ± 0.009	1.191 ± 0.021	1.508 ± 0.029	0.795 ± 0.041	
80.5	13.93	1.014	0.159 ± 0.005	0.330 ± 0.010	0.973 ± 0.026	0.342 ± 0.028	4.242 ± 0.300
88.5	14.31	0.992	0.101 ± 0.003	0.215 ± 0.006	0.966 ± 0.007	0.224 ± 0.013	1.313 ± 0.052
96.5	14.68	0.971	0.061 ± 0.002	0.133 ± 0.004	0.810 ± 0.023	0.166 ± 0.014	1.084 ± 0.046
112	15.43	1.086	2.647 ± 0.036	5.151 ± 0.070	2.507 ± 0.054	2.070 ± 0.105	15.755 ± 0.432
128.5	17.61	0.970	1.033 ± 0.015	2.233 ± 0.033	1.554 ± 0.016	1.450 ± 0.052	11.781 ± 0.392
136.5	18.30	1.003	2.048 ± 0.030	4.321 ± 0.064	2.150 ± 0.039	2.028 ± 0.095	12.817 ± 0.237
152.5	19.36	1.023	1.251 ± 0.021	2.582 ± 0.044	1.940 ± 0.039	1.344 ± 0.070	9.189 ± 0.197
168.5	20.43	1.012	0.682 ± 0.012	1.434 ± 0.026	0.949 ± 0.012	1.527 ± 0.066	10.225 ± 0.316
184.5	23.04	0.985	1.280 ± 0.020	2.762 ± 0.043	2.385 ± 0.072	1.172 ± 0.080	24.724 ± 0.829
200.5	25.41	0.987	1.934 ± 0.028	4.099 ± 0.060	1.777 ± 0.043	2.336 ± 0.132	17.374 ± 0.354
208.5	26.15	0.965	1.219 ± 0.017	2.660 ± 0.038	1.855 ± 0.045	1.453 ± 0.081	12.758 ± 0.281
218.5	27.05	0.978	0.252 ± 0.007	0.539 ± 0.015	0.709 ± 0.006	0.771 ± 0.045	
232.5	28.54	1.015	0.025 ± 0.001	0.051 ± 0.002	0.692 ± 0.007	0.074 ± 0.006	0.717 ± 0.046
248.5	34.55	0.964	0.032 ± 0.001	0.070 ± 0.002	0.590 ± 0.005	0.120 ± 0.008	0.989 ± 0.067
256.5	35.79	1.012	0.075 ± 0.002	0.153 ± 0.005	1.323 ± 0.036	0.118 ± 0.010	0.899 ± 0.034
264.5	37.57	0.950	0.048 ± 0.001	0.105 ± 0.003	1.178 ± 0.021	0.091 ± 0.006	1.762 ± 0.165
271	39.56	0.956	0.028 ± 0.001	0.062 ± 0.002	1.372 ± 0.017	0.046 ± 0.003	
273	40.13	0.955	0.023 ± 0.001	0.051 ± 0.002	1.233 ± 0.017	0.043 ± 0.003	2.401 ± 0.602
275	40.70	0.986	0.037 ± 0.001	0.079 ± 0.003	1.372 ± 0.034	0.058 ± 0.005	
277	41.33	0.955	0.333 ± 0.007	0.729 ± 0.016	1.426 ± 0.009	0.522 ± 0.023	
279	41.89	0.983	0.862 ± 0.014	1.846 ± 0.031	1.366 ± 0.024	1.380 ± 0.066	
281	42.34	0.967	0.968 ± 0.017	2.084 ± 0.037	1.293 ± 0.025	1.646 ± 0.086	
283	42.79	0.986	1.560 ± 0.024	3.333 ± 0.051	1.531 ± 0.035	2.224 ± 0.121	
285	43.35	0.996	1.941 ± 0.027	4.085 ± 0.058	1.860 ± 0.010	2.244 ± 0.067	
287	44.02	0.970	2.126 ± 0.031	4.584 ± 0.069	1.880 ± 0.015	2.492 ± 0.083	
289	44.69	0.998	2.227 ± 0.031	4.658 ± 0.067	2.081 ± 0.020	2.288 ± 0.078	
291	45.37	0.990	1.951 ± 0.030	4.135 ± 0.064	1.878 ± 0.010	2.252 ± 0.072	
293	46.04	0.999	1.689 ± 0.024	3.542 ± 0.051	1.790 ± 0.021	2.025 ± 0.074	
295	46.71	0.981	1.465 ± 0.021	3.134 ± 0.046	1.682 ± 0.007	1.907 ± 0.057	7.649 ± 0.165
304.5	49.00	0.977	0.993 ± 0.015	2.133 ± 0.033	0.990 ± 0.015	2.208 ± 0.095	21.963 ± 1.496
320.5	51.65	0.985	0.190 ± 0.006	0.405 ± 0.014	0.936 ± 0.008	0.444 ± 0.030	1.612 ± 0.046
336.5	53.84	0.974	2.280 ± 0.032	4.900 ± 0.070	2.003 ± 0.052	2.512 ± 0.149	25.388 ± 0.973
344.5	54.87	0.975	1.675 ± 0.024	3.610 ± 0.052	1.834 ± 0.032	2.023 ± 0.091	19.291 ± 0.837
352.5	55.89	0.980	2.183 ± 0.030	4.684 ± 0.067	1.977 ± 0.051	2.437 ± 0.143	18.556 ± 0.648
360.5	57.14	0.986	1.607 ± 0.023	3.438 ± 0.052	1.693 ± 0.013	2.089 ± 0.068	8.181 ± 0.145
368.5	59.01	0.998	0.141 ± 0.002	0.293 ± 0.005	0.812 ± 0.013	0.372 ± 0.017	2.325 ± 0.092
384.5	61.05	0.975	0.116 ± 0.003	0.247 ± 0.008	0.851 ± 0.010	0.299 ± 0.019	1.545 ± 0.066
392.5	62.07	0.976	0.148 ± 0.004	0.320 ± 0.010	0.920 ± 0.009	0.359 ± 0.022	2.133 ± 0.084
400.5	63.09	0.969	0.086 ± 0.003	0.186 ± 0.006	0.861 ± 0.024	0.223 ± 0.019	1.712 ± 0.098
408.5	64.88	1.002	0.110 ± 0.003	0.229 ± 0.007	0.925 ± 0.004	0.256 ± 0.016	1.916 ± 0.097
416.5	67.06	0.992	0.119 ± 0.003	0.250 ± 0.007	0.811 ± 0.005	0.319 ± 0.018	6.284 ± 0.929
418	67.61	0.986	0.071 ± 0.002	0.151 ± 0.005	0.621 ± 0.004	0.251 ± 0.015	
420	68.16	0.973	0.098 ± 0.003	0.210 ± 0.006	0.832 ± 0.016	0.261 ± 0.018	
422	68.70	0.978	0.103 ± 0.003	0.220 ± 0.006	0.847 ± 0.018	0.268 ± 0.018	1.934 ± 0.096
437	74.35	0.956	1.438 ± 0.022	3.164 ± 0.051	1.517 ± 0.027	2.164 ± 0.103	
440.5	75.62	0.979	1.888 ± 0.027	4.025 ± 0.061	1.809 ± 0.050	2.310 ± 0.144	4.189 ± 0.065
456.5	78.58	1.002	2.212 ± 0.032	4.653 ± 0.070	1.844 ± 0.034	2.624 ± 0.123	12.908 ± 0.292
472.5	81.21	0.974	0.283 ± 0.006	0.606 ± 0.014	1.331 ± 0.008	0.474 ± 0.022	3.461 ± 0.133
504.5	87.96	0.954	0.066 ± 0.001	0.144 ± 0.003	0.793 ± 0.009	0.189 ± 0.008	3.166 ± 0.548
520.5	92.17	0.973	0.788 ± 0.013	1.708 ± 0.031	1.521 ± 0.021	1.176 ± 0.052	17.334 ± 1.213
536.5	94.76	0.973	0.116 ± 0.003	0.248 ± 0.007	0.839 ± 0.011	0.310 ± 0.018	1.558 ± 0.073
552.5	97.35	1.000	0.058 ± 0.002	0.122 ± 0.004	0.798 ± 0.005	0.160 ± 0.010	0.743 ± 0.033
568.5	99.94	0.993	0.067 ± 0.002	0.140 ± 0.004	0.774 ± 0.007	0.191 ± 0.012	1.355 ± 0.096
584.5	102.62	0.990	0.075 ± 0.002	0.160 ± 0.005	0.841 ± 0.009	0.200 ± 0.013	0.867 ± 0.035
590	104.15	0.994	0.051 ± 0.002	0.107 ± 0.004	0.705 ± 0.007	0.160 ± 0.011	
600	107.33	0.974	1.051 ± 0.015	2.271 ± 0.035	1.302 ± 0.006	1.840 ± 0.057	17.365 ± 0.764
616.5	112.56	0.991	0.401 ± 0.007	0.849 ± 0.015	1.068 ± 0.025	0.841 ± 0.048	2.025 ± 0.053
632.5	116.84	0.990	0.496 ± 0.008	1.054 ± 0.019	1.123 ± 0.010	0.995 ± 0.038	4.881 ± 0.174
648.5	119.84	0.989	1.361 ± 0.020	2.899 ± 0.045	1.476 ± 0.025	2.085 ± 0.094	
664.5	122.96	0.990	0.127 ± 0.004	0.270 ± 0.009	0.771 ± 0.012	0.372 ± 0.025	1.204 ± 0.041
680.5	126.77	0.974	0.079 ± 0.002	0.171 ± 0.005	0.782 ± 0.003	0.233 ± 0.014	
704.5	131.75	0.976	0.290 ± 0.007	0.627 ± 0.015	1.338 ± 0.023	0.501 ± 0.029	
720.5	134.25	0.991	0.488 ± 0.010	1.036 ± 0.022	1.051 ± 0.014	1.054 ± 0.050	
736.5	136.17	0.992	0.460 ± 0.008	0.977 ± 0.019	0.956 ± 0.017	1.094 ± 0.057	
Mean ± std. dev.			0.771 ± 0.823	1.639 ± 1.739	1.331 ± 0.561	1.009 ± 0.859	6.941 ± 7.037
Mean ± SDOM				1.639 ± 0.202	1.331 ± 0.065	1.009 ± 0.100	6.941 ± 0.985
Replicate measurements[b]							
16.5	9.683	0.973	0.790 ± 0.015	1.708 ± 0.032	1.973 ± 0.023	0.870 ± 0.038	6.605 ± 0.161
184.5	23.041	0.987	1.315 ± 0.022	2.806 ± 0.047	2.578 ± 0.062	1.101 ± 0.064	25.112 ± 0.844
Blank			(x 10^{-11})				
bk1			0.00071				
bk2			0.00120				
bk3			0.00089				
bk4			0.00148				
bk5			0.00067				
bk6			0.00053				

[a]normalisation using $^{230}Th_{xs}$ (see Nuttin and Hillaire-Marcel, 2015 for $^{230}Th_{xs}$ results)

[b]new leachates

*2-sigma uncertainties.

Table2

Table 2. Correlation coefficients of Be isotopes (concentration, ratio and fluxes) and sedimentological parameters.

Parameters	^{9}Be (at./g)	^{10}Be (at./g)	Rapport ^{10}Be/^{9}Be	$^{230}(Th_{xs})^{0}$ (dpm.g^{-1})	Flux-^{10}Be Th_norm. (atoms.cm^{-2}.kyr^{-1}	PC1	PC2
SAR 170714B (cm/kyr)	n.s.	n.s.	n.s.	n.s.	n.s.	n.s.	n.s.
XRD- Quartz (%)	0.51	0.50	0.49	n.s.	0.49	-0.68	n.s.
XRD- K-Feldspar (%)	0.55	0.69	0.75	n.s.	0.66	-0.77	n.s.
XRD- Plagioclase (%)	0.54	0.72	0.80	n.s.	0.71	-0.84	n.s.
XRD- Calcite (%)	-0.62	-0.72	-0.76	n.s.	-0.66	0.80	n.s.
XRD- Dolomite (%)	-0.51	-0.68	-0.74	n.s.	-0.71	0.89	n.s.
XRF- Ca/Fe	-0.73	-0.80	-0.81	0.55	-0.68	0.95	n.s.
XRF- K/Ti	-0.66	-0.74	-0.77	0.42	-0.65	0.85	n.s.
XRF- Ti/Ca	0.71	0.78	0.79	0.51	0.67	-0.94	n.s.
XRF- Ca	-0.71	-0.78	-0.77	0.54	-0.66	0.92	n.s.
XRF- Fe	0.69	0.77	0.81	0.53	0.66	-0.91	n.s.
GS- 0-2 µm (%)	n.s.	n.s.	0.40	n.s.	0.39	-0.58	0.74
GS- 2-4 µm (%)	0.73	0.77	0.72	0.51	0.61	-0.86	0.47
GS- 4-8 µm (%)	0.79	0.78	0.67	0.62	0.55	-0.82	0.48
GS- 8-63 µm (%)	n.s.	n.s.	n.s.	0.00	n.s.	n.s.	n.s.
GS- >63 µm (%)	-0.70	-0.73	-0.63	0.61	-0.51	0.76	-0.50
Density (g.cm^{-3})	-0.77	-0.76	-0.73	0.58	-0.66	0.77	n.s.
^{9}Be (at)	**1.00**	0.88	0.71	0.72	0.60	-0.81	n.s.
^{10}Be (at)	0.88	**1.00**	0.94	0.68	0.73	-0.89	n.s.
Ratio ^{10}Be/^{9}Be	0.71	0.94	**1.00**	0.50	0.81	-0.88	n.s.
$^{230}(Th_{xs})^{0}$ (dpm.g^{-1})	0.72	0.68	0.50	**1.00**	n.s.	-0.54	n.s.
Flux-^{10}Be sed. (atoms.cm^{-2}kyr^{-1})	0.60	0.73	0.81	n.s.	**1.00**	-0.75	n.s.
PC1 Sedimentological parameter	-0.81	-0.89	-0.88	-0.54	-0.71		
PC2 Sedimentological parameter	n.s.	n.s.	n.s.	n.s.	n.s.		

n.s. are not significants ($P < 0.001$)

Table3

Table 3. ^{10}Be-production/flux in litterature (in atoms.cm^{-2}.kyr^{-1})

Range (x 10^8)	Mean values (x 10^8	Notes	References
^{10}Be-production			
5.7 - 10		Global average ^{10}Be-production (model)	*Webber et al., 2007; Masarik and Beer, 1999, 2009; Kovaltsov and Usoskin, 2010*
12 - 19		60-90°N ^{10}Be-production (model)	
	6.6	Global average ^{10}Be-production (model)	*Masarik and Beer, 2009*
5.2 - 26.4	12.1	Global average ^{10}Be-production (analytical)	*Monaghan et al., 1986 (from precipitation measurements during the year 1980)*
11 - 17	14.0	Long term averaged glob. av. ^{10}Be-prod. (analytical)	
			Webber and Higbie, 2003; Webber et al., 2007
	6.0	Global average ^{10}Be-production (model)	
	14.2	Global average ^{10}Be-production (empiric)	*Lal and Peters, 1967*
	9.5	Global average ^{10}Be-production (analytical)	*O'Brien, 1979; O'Brien et al., 1991*
	12.6	Global average ^{10}Be-production (empiric)	*Lal, 1988*
^{10}Be-flux in ice-core records			
1.8 - 8.6	3.4	Greenland Summit (GRIP/GISP2)	*Muscheler et al., 2005; Finkel and Nishiizumi, 199*
	3.3	Dye 3 (Greenland)	*Beer et al., 1991*
1.5 - 12.8		Renland Ice Core over 1931-1987 (Greenland)	Aldahan et al., 1998
1.4 - 10		Dronning Maud Land ice core over 1932-1988 (Antarctic	
	4.0±0.3	EPICA DML (Neumayer surface snow, Antarctic)	Auer et al., 2009
	1.9±0.1	EPICA DML (Kohnen deep ice core, Antarctic)	
	1.4±0.2	Dome C (surface firn and firn core 0-12 m; Antarctica)	
1.2 - 2.5		Epica DC between 320-340 kyr	Cauquoin et al., 2014
0.6 - 3.3	1.6	Epica DC between 200-800 kyr	Cauquoin, 2013
	2.5	Vostok, South Pole (Antarctic)	*Raisbeck and Yiou, 1985*
	1.4	Taylor Dome (Antarctic)	*Steig et al., 1996*
	1.7 and 1.8	Concordia and Vostok over the last 60 years (Antarctic)	*Baroni et al., 2011*
	4.8±1.6	Law Dome snow pit over the year 2001 (Antarctic)	Pedro et al., 2006
2.0 - 4.5		Dome Fuji ice core over 700-1900 yr CE (Antarctica)	Horiuchi et al., 2008
	2.2 (2.3)	GRIP snow pit (Greenland) ^{10}Be deposition flux (1986-19	*Heikkilä et al., 2008*
	2.8	ECHAM5-HAM general circulation model ^{10}Be deposition	
^{10}Be-flux in marine records			
8.2 - 31.1	16.3	ODP1063 (Bermuda Rise): 0-250 kyr BP	*Christl et al., 2007, 2010*
7.8 - 37.1	16.1	ODP983 (North Atlantic): 0-250 kyr BP	
9 - 28		Globally intergrated / long-term averaged ^{10}Be-fluxes	
15 - 35		ODP 1063A (Bermuda Rise): 170-200 kyr BP, IB exc.	*Knudsen et al., 2008*
10 - 70		ODP 983B (North Atlantic): 170-200 kyr BP, IB exc.	
5 - 27		ODP 925 (Ceara Rise): 0-7 Ma	*Murayama et al., 1997*
5 - 60		Globally stacked deep-sea sediments: 0-200 kyr BP	Frank et al., 1997
6 - 7		ACEX average ^{10}Be-flux for the past 12.3 Ma (Actic)	Frank et al., 2008
31.9 - 65.9	40.9	Portuguese Margin (20-45 kyr BP)	*Ménabréaz et al., 2011*
2 - 23		Four Arctic Ocean cores (F=C x S x D)	*Eisenhauer et al., 1994; Aldahan et al., 1997*
^{10}Be-flux in PC16 (Baffin Bay marine sediments)			
0.7 - 25.4 (1 - 35.5)	6.9 (9.7)	(values corrected)*	*This study*
fluxes by facies:			
6.5 - 8.6 (9.1 - 12)	7.6 (10.7)	Facies UB (Holocene)	
0.7 - 6.3 (1 - 8.8)	2 (2.8)	Facies BBDC (coarse carbonate-rich sediments)	
4.2 - 25.4 (5.8 - 35.5)	14.5 (20.2)	Facies LDC (fine feldspar-rich sediments)	
9.2 - 24.7 (12.8 - 34.6)	14.1 (19.8)	Facies OC (very fine feldspar-rich sediments)	

*correction to encompass the underestimation of the flux due to methodological biais, see text for details

Figure

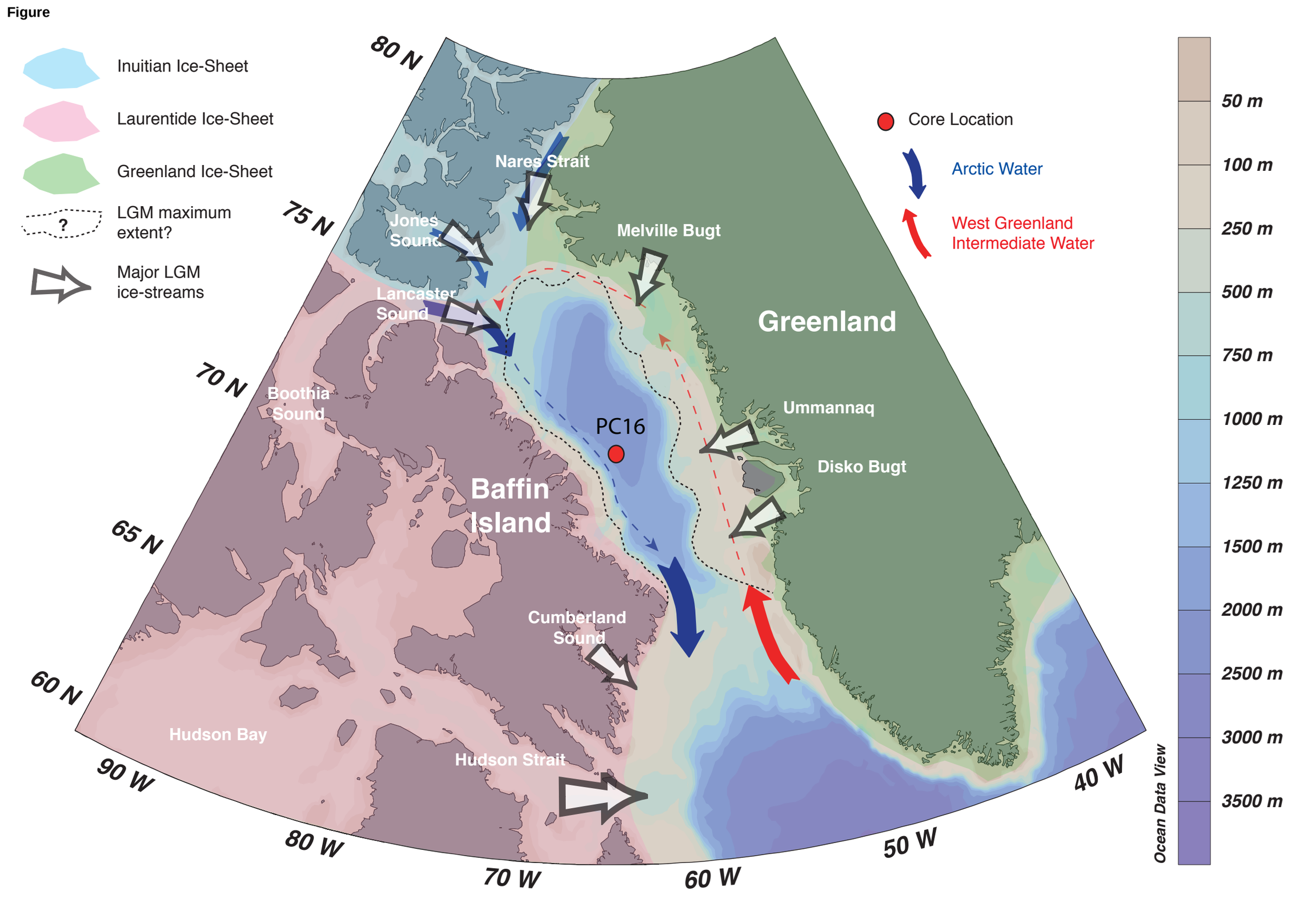
Inuitian Ice-Sheet
Laurentide Ice-Sheet
Greenland Ice-Sheet
LGM maximum extent?
Major LGM ice-streams
Core Location
Arctic Water
West Greenland Intermediate Water
80 N
75 N
70 N
65 N
60 N
90 W
80 W
70 W
60 W
50 W
40 W
Nares Strait
Jones Sound
Lancaster Sound
Melville Bugt
Greenland
Boothia Sound
PC16
Ummannaq
Disko Bugt
Baffin Island
Cumberland Sound
Hudson Bay
Hudson Strait
50 m
100 m
250 m
500 m
750 m
1000 m
1250 m
1500 m
2000 m
2500 m
3000 m
3500 m
Ocean Data View

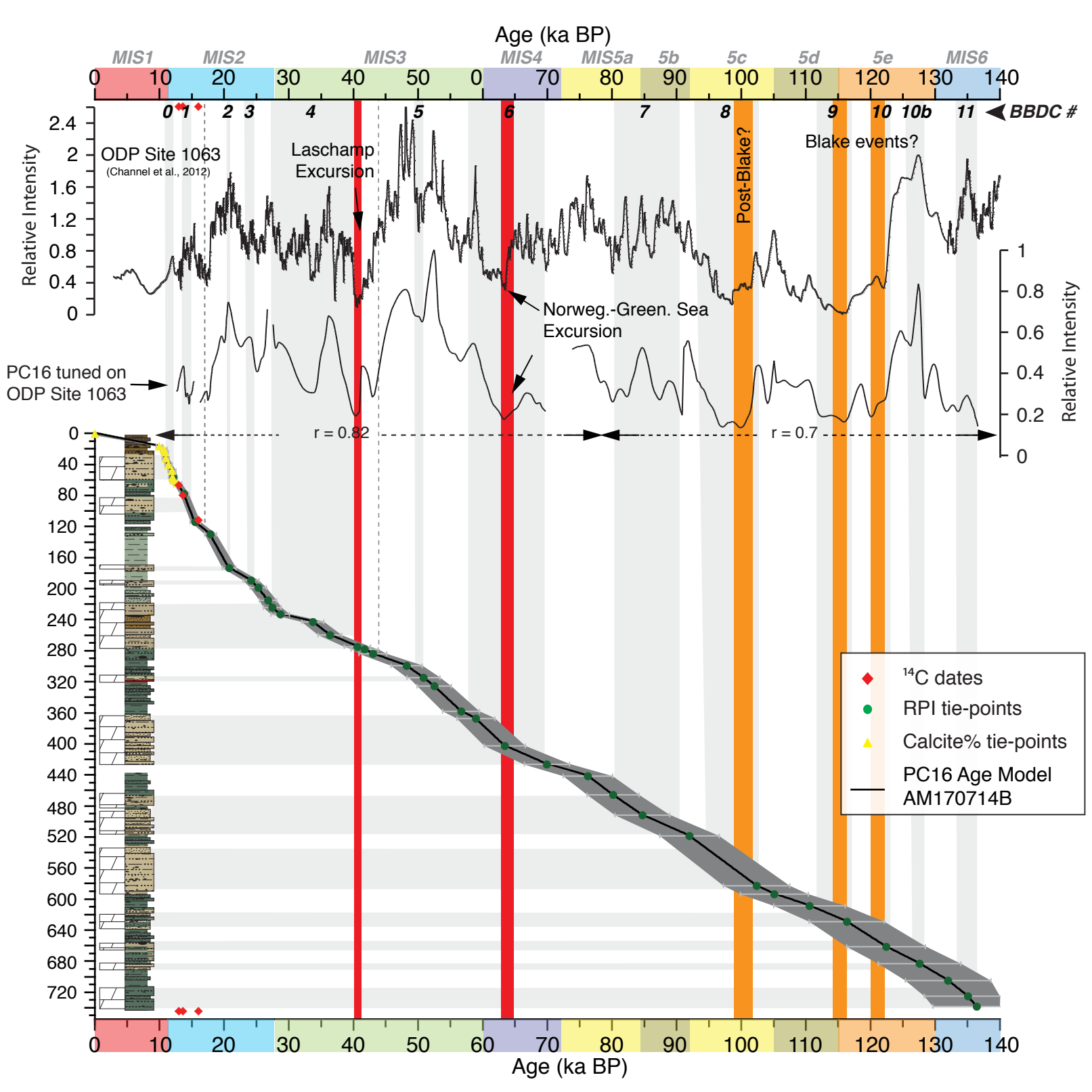
Age (ka BP)
MIS1
MIS2
MIS3
MIS4
MIS5a
5b
5c
5d
5e
MIS6
0 10 20 30 40 50 0 70 80 90 100 110 120 130 140
0 1 2 3 4 5 6 7 8 9 10 10b 11 BBDC #
Relative Intensity
2.4 2 1.6 1.2 0.8 0.4 0
ODP Site 1063
(Channel et al., 2012)
Laschamp
Excursion
Post-Blake?
Blake events?
Norweg.-Green. Sea
Excursion
PC16 tuned on
ODP Site 1063
1 0.8 0.6 0.4 0.2 0
Relative Intensity
r = 0.82
r = 0.7
0 40 80 120 160 200 240 280 320 360 400 440 480 520 560 600 640 680 720
14C dates
RPI tie-points
Calcite% tie-points
PC16 Age Model
AM170714B
0 10 20 30 40 50 60 70 80 90 100 110 120 130 140
Age (ka BP)

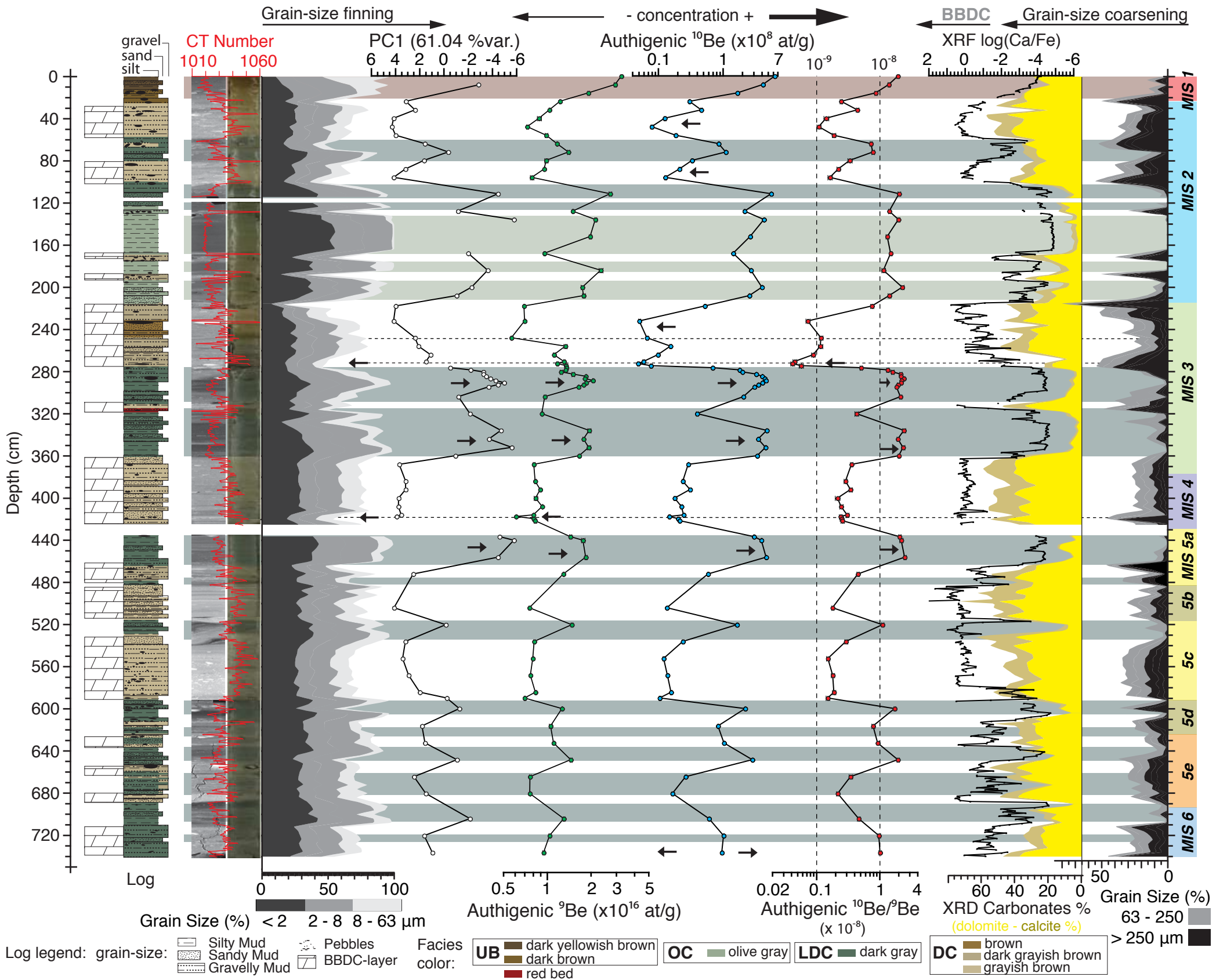
Grain-size finning
- concentration +
BBDC
Grain-size coarsening
gravel
sand
silt
CT Number
1010
1060
PC1 (61.04 %var.)
6 4 2 0 -2 -4 -6
Authigenic ^{10}Be (x10^{8} at/g)
0.1 1 7
10^{-9}
10^{-8}
XRF log(Ca/Fe)
2 0 -2 -4 -6
Depth (cm)
0 40 80 120 160 200 240 280 320 360 400 440 480 520 560 600 640 680 720
MIS 1
MIS 2
MIS 3
MIS 4
MIS 5a
5b
5c
5d
5e
MIS 6
Log
0 50 100
Grain Size (%) < 2 2 - 8 8 - 63 µm
0.5 1 2 3 5
Authigenic ^{9}Be (x10^{16} at/g)
0.02 0.1 1 4
Authigenic ^{10}Be/^{9}Be
(x 10^{-8})
60 40 20 0
XRD Carbonates %
(dolomite - calcite %)
50 0
Grain Size (%)
63 - 250
> 250 µm
Log legend: grain-size:
Silty Mud
Sandy Mud
Gravelly Mud
Pebbles
BBDC-layer
Facies color:
UB
dark yellowish brown
dark brown
red bed
OC
olive gray
LDC
dark gray
DC
brown
dark grayish brown
grayish brown

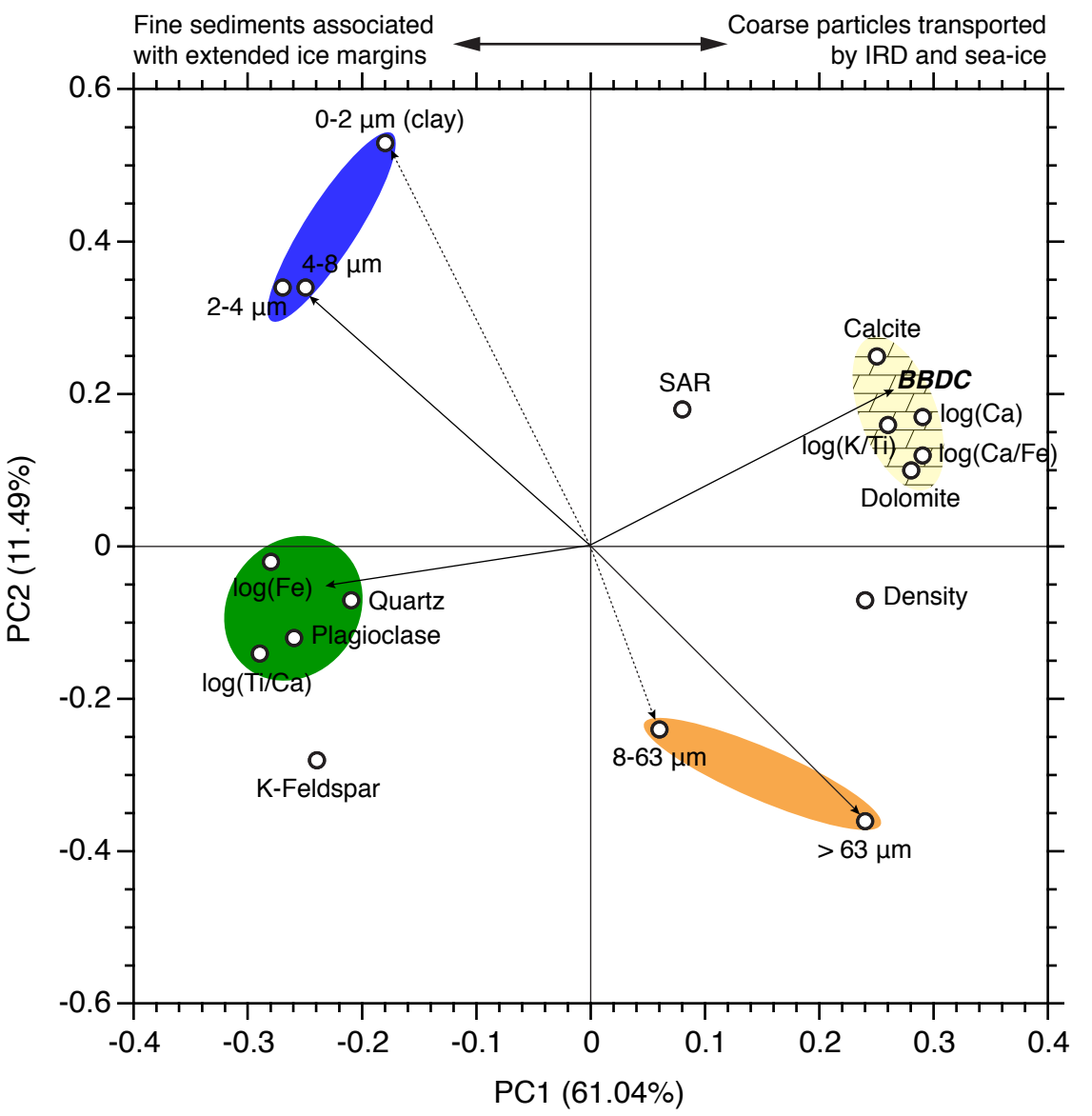
Fine sediments associated with extended ice margins
Coarse particles transported by IRD and sea-ice
0-2 µm (clay)
4-8 µm
2-4 µm
SAR
Calcite
BBDC
log(Ca)
log(K/Ti)
log(Ca/Fe)
Dolomite
log(Fe)
Quartz
Plagioclase
log(Ti/Ca)
K-Feldspar
Density
8-63 µm
> 63 µm
PC2 (11.49%)
PC1 (61.04%)
0.6
0.4
0.2
0
-0.2
-0.4
-0.6
-0.4
-0.3
-0.2
-0.1
0
0.1
0.2
0.3
0.4

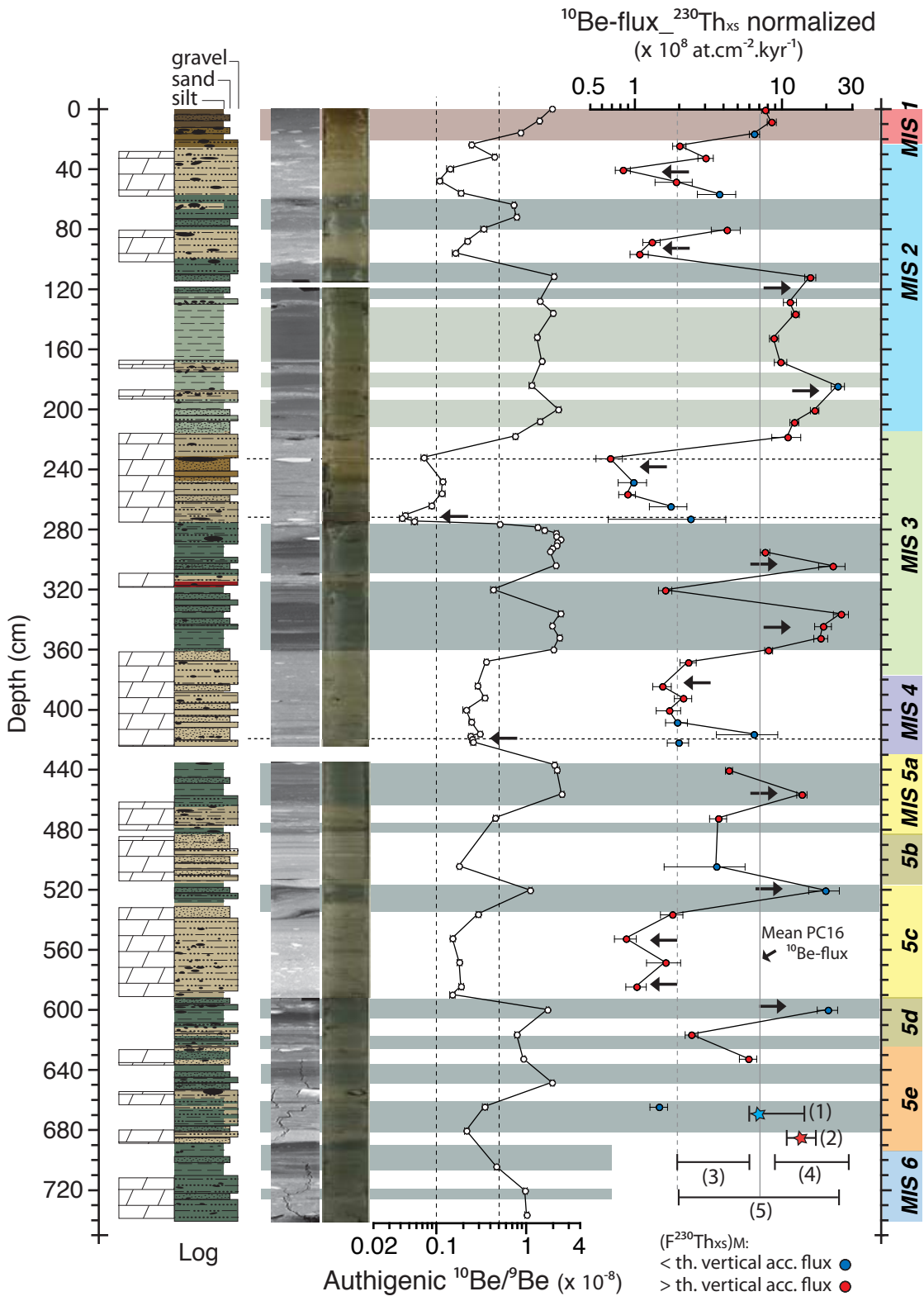
^{10}Be-flux_^{230}Th$_{xs}$ normalized
(x 10^{8} at.cm^{-2}.kyr^{-1})
0.5
1
10
30
gravel
sand
silt
Depth (cm)
0
40
80
120
160
200
240
280
320
360
400
440
480
520
560
600
640
680
720
MIS 1
MIS 2
MIS 3
MIS 4
MIS 5a
5b
5c
5d
5e
MIS 6
Mean PC16
^{10}Be-flux
(1)
(2)
(3)
(4)
(5)
Log
0.02
0.1
1
4
Authigenic ^{10}Be/^{9}Be (x 10^{-8})
(F^{230}Th$_{xs}$)M:
< th. vertical acc. flux
> th. vertical acc. flux

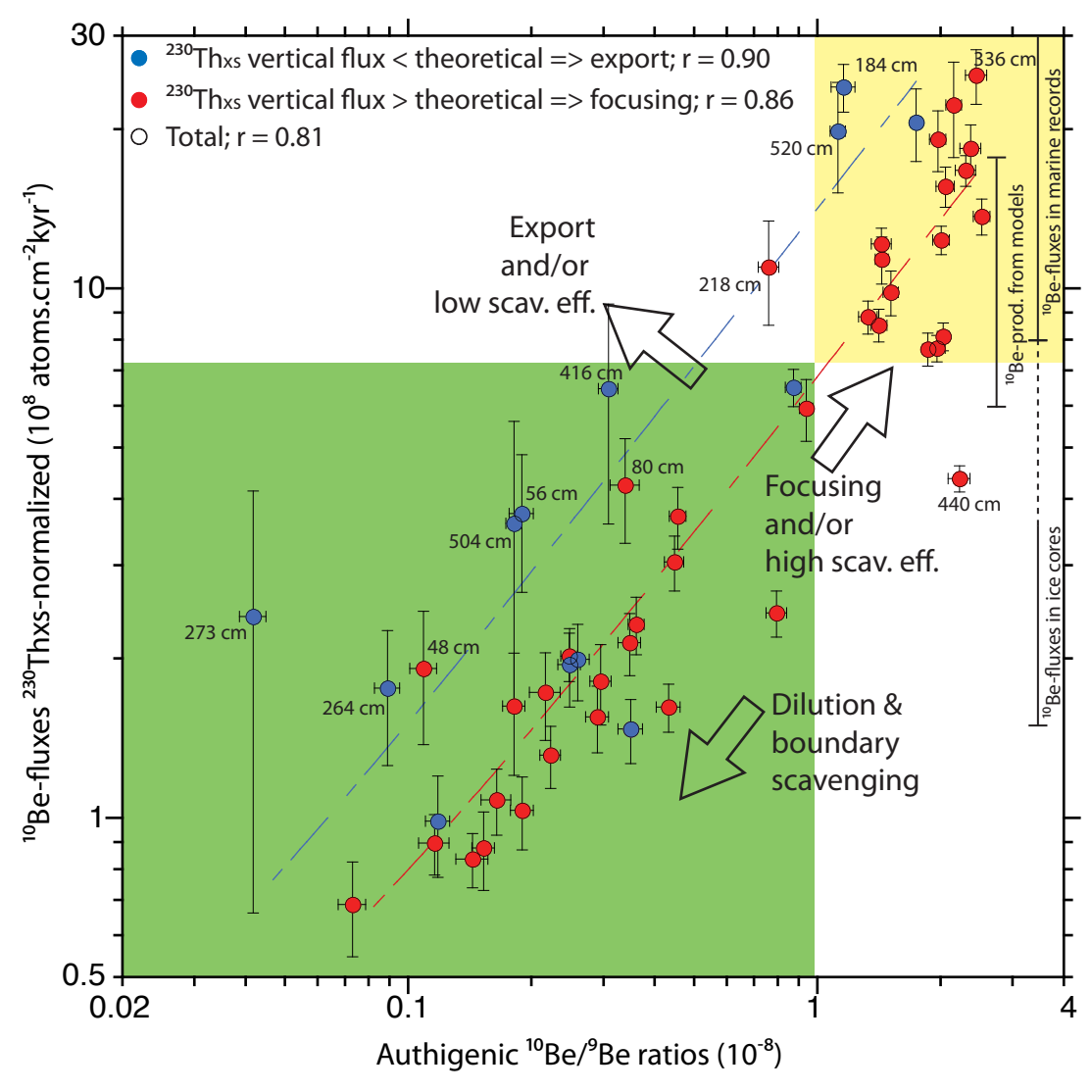
230Thxs vertical flux < theoretical => export; r = 0.90
230Thxs vertical flux > theoretical => focusing; r = 0.86
Total; r = 0.81
Export and/or low scav. eff.
Focusing and/or high scav. eff.
Dilution & boundary scavenging
184 cm
336 cm
520 cm
218 cm
416 cm
80 cm
56 cm
504 cm
440 cm
273 cm
48 cm
264 cm
10Be-prod. from models
10Be-fluxes in marine records
10Be-fluxes in ice cores
10Be-fluxes 230Thxs-normalized (10^8 atoms.cm^-2kyr^-1)
Authigenic 10Be/9Be ratios (10^-8)
30
10
1
0.5
0.02
0.1
1
4

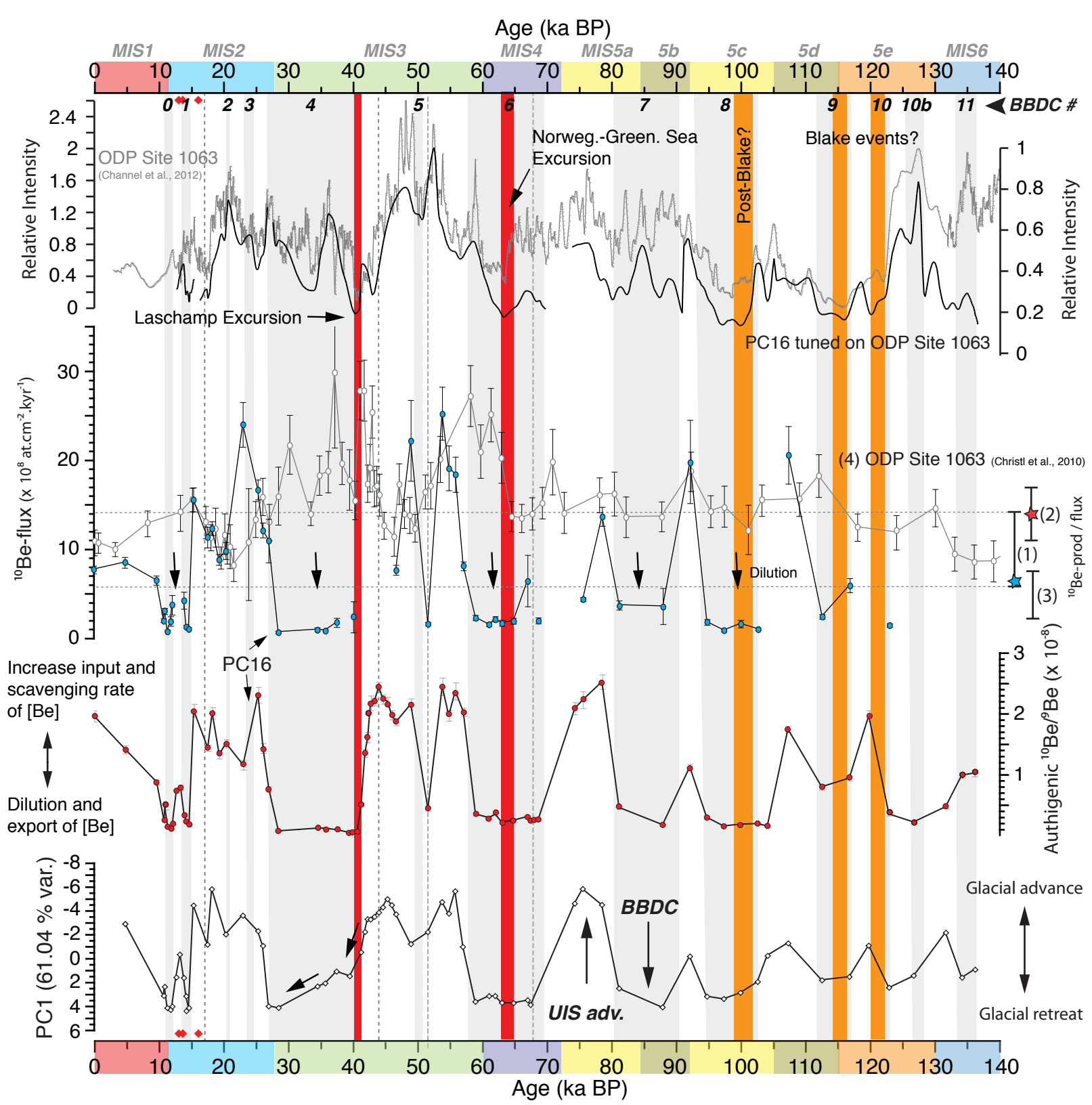
Age (ka BP)
MIS1
MIS2
MIS3
MIS4
MIS5a
5b
5c
5d
5e
MIS6
0 10 20 30 40 50 60 70 80 90 100 110 120 130 140
0 1 2 3 4 5 6 7 8 9 10 10b 11 BBDC #
Relative Intensity
ODP Site 1063
(Channel et al., 2012)
Norweg.-Green. Sea Excursion
Post-Blake?
Blake events?
Laschamp Excursion
PC16 tuned on ODP Site 1063
^{10}Be-flux (x 10^{8} at.cm^{-2}.kyr^{-1})
(4) ODP Site 1063 (Christl et al., 2010)
Dilution
(1)
(2)
(3)
^{10}Be-prod / flux
PC16
Increase input and scavenging rate of [Be]
Dilution and export of [Be]
Authigenic ^{10}Be/^{9}Be (x 10^{-8})
PC1 (61.04 % var.)
BBDC
UIS adv.
Glacial advance
Glacial retreat
Age (ka BP)

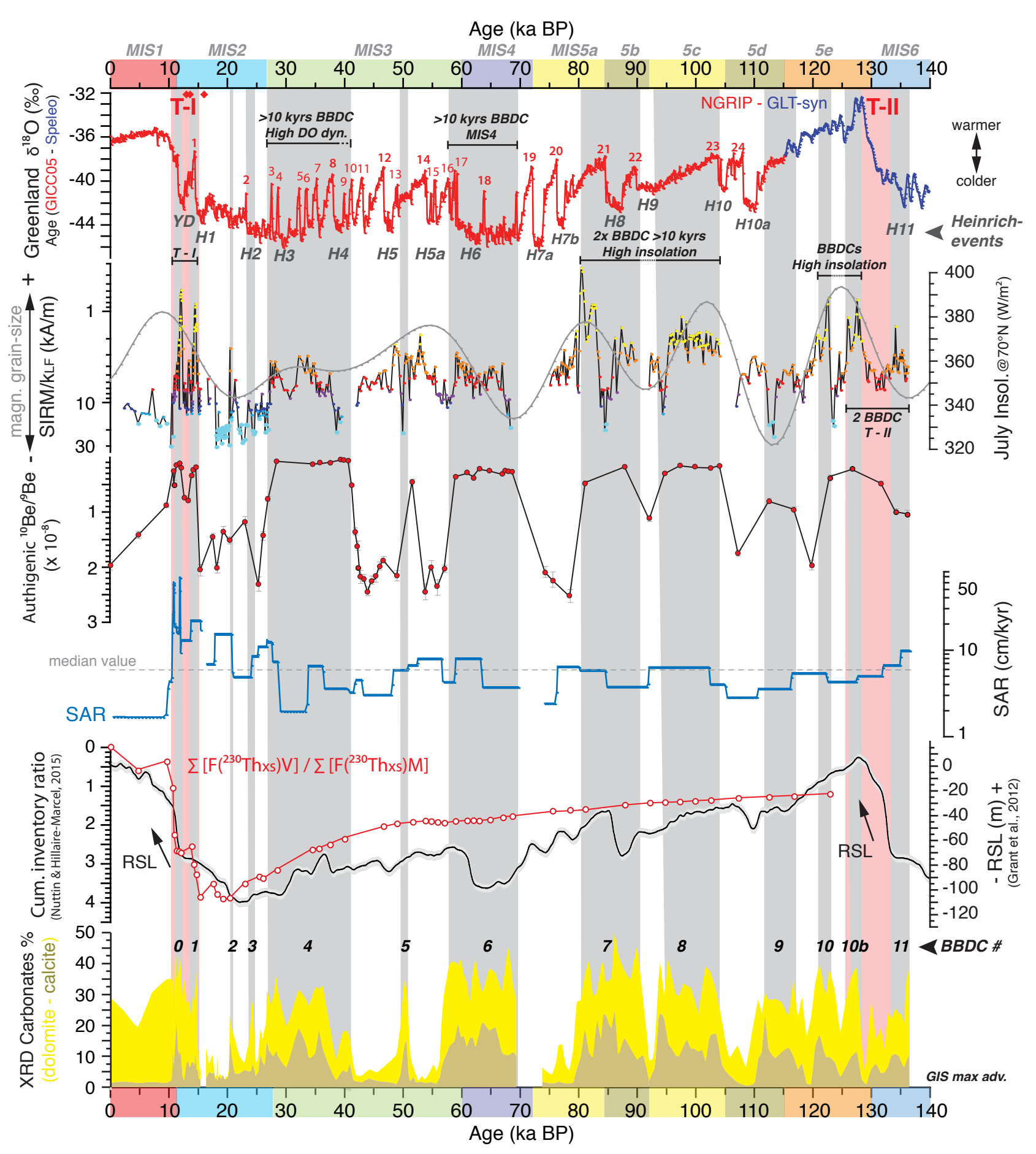
Age (ka BP)
MIS1
MIS2
MIS3
MIS4
MIS5a
5b
5c
5d
5e
MIS6
Greenland δ18O (‰)
Age (GICC05 - Speleo)
NGRIP - GLT-syn
T-I
T-II
warmer
colder
>10 kyrs BBDC
High DO dyn.
>10 kyrs BBDC
MIS4
YD
H1
H2
H3
H4
H5
H5a
H6
H7a
H7b
H8
H9
H10
H10a
H11
Heinrich-events
T - I
2x BBDC >10 kyrs
High insolation
BBDCs
High insolation
2 BBDC
T - II
magn. grain-size
SIRM/kLF (kA/m)
July Insol.@70°N (W/m²)
Authigenic 10Be/9Be
(x 10-8)
median value
SAR
SAR (cm/kyr)
Cum. inventory ratio
(Nuttin & Hillaire-Marcel, 2015)
Σ [F(230Thxs)V] / Σ [F(230Thxs)M]
RSL
- RSL (m) +
(Grant et al., 2012)
XRD Carbonates %
(dolomite - calcite)
BBDC #
GIS max adv.

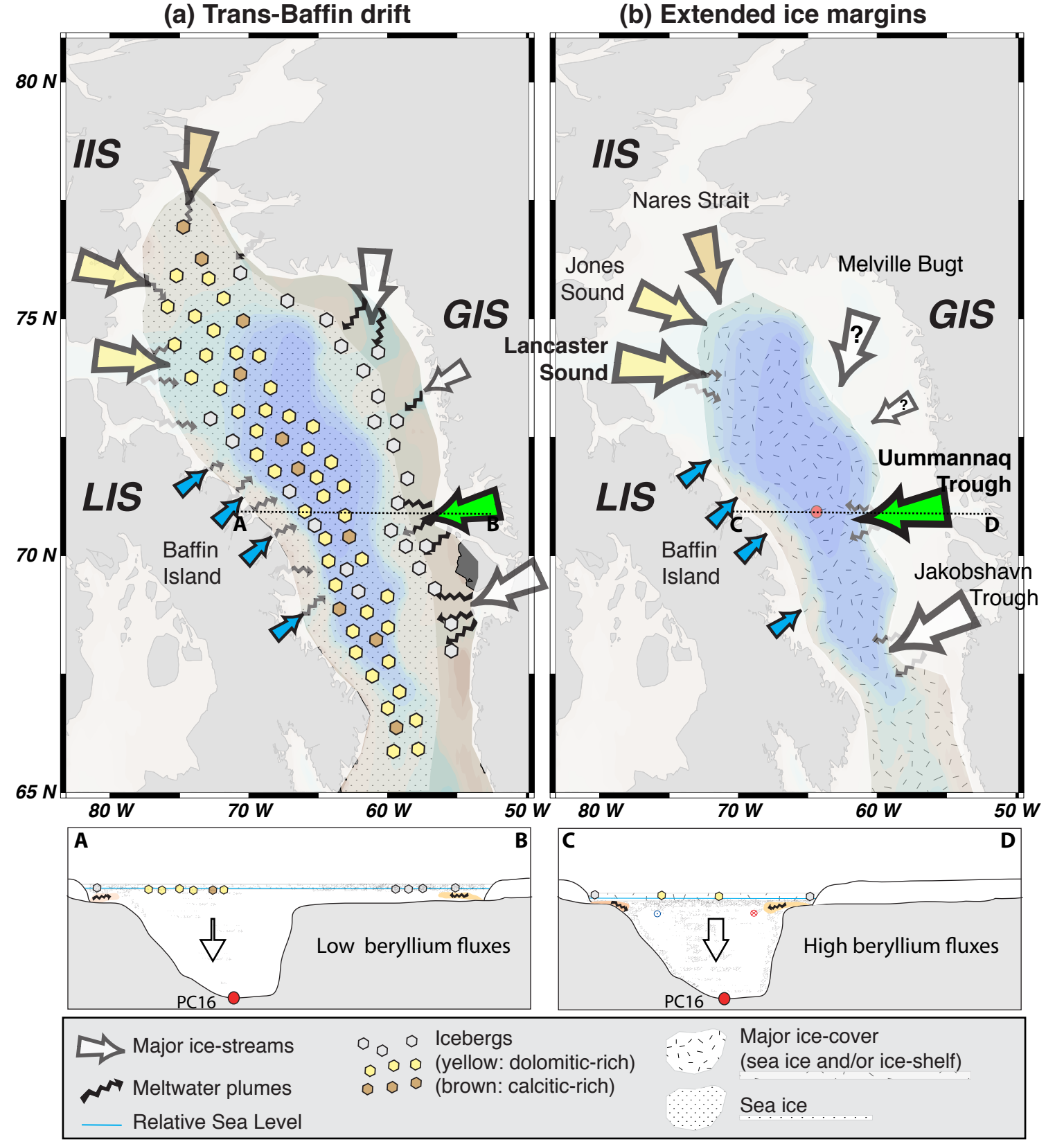
(a) Trans-Baffin drift
(b) Extended ice margins
80 N
75 N
70 N
65 N
80 W
70 W
60 W
50 W
IIS
GIS
LIS
Baffin Island
A
B
Nares Strait
Jones Sound
Melville Bugt
Lancaster Sound
Uummannaq Trough
Jakobshavn Trough
C
D
?
A
B
Low beryllium fluxes
PC16
C
D
High beryllium fluxes
PC16
Major ice-streams
Meltwater plumes
Relative Sea Level
Icebergs
(yellow: dolomitic-rich)
(brown: calcitic-rich)
Major ice-cover
(sea ice and/or ice-shelf)
Sea ice